Acta Pharmaceutica Sinica B 2025;15(4):2217−2236

Chinese Pharmaceutical Association
Institute of Materia Medica, Chinese Academy of Medical Sciences

Acta Pharmaceutica Sinica B

www.elsevier.com/locate/apsb
www.sciencedirect.com

ORIGINAL ARTICLE

Intranodal injection of neoantigen-bearing engineered *Lactococcus lactis* triggers epitope spreading and systemic tumor regressions

Junmeng Zhu[a,b], Yi Sun[a,b], Xiaoping Qian[a,b], Lin Li[c,d], Fangcen Liu[d], Xiaonan Wang[a,b], Yaohua Ke[a,b], Jie Shao[b,c], Lijing Zhu[a,b], Lifeng Wang[a,b], Qin Liu[a,b,*], Baorui Liu[a,b,c,*]

[a]*The Comprehensive Cancer Centre, Nanjing Drum Tower Hospital, Affiliated Hospital of Medical School, Nanjing University, Nanjing 210008, China*
[b]*The Clinical Cancer Institute of Nanjing University, Nanjing 210008, China*
[c]*Department of Oncology, Nanjing Drum Tower Hospital Clinical College of Nanjing University of Chinese Medicine, Nanjing 210008, China*
[d]*Department of Pathology, The Affiliated Hospital of Nanjing University Medical School, Nanjing 210008, China*

Received 20 August 2024; received in revised form 25 November 2024; accepted 15 December 2024

KEY WORDS

Synthetic biology;
Probiotic;
Cell-penetrating peptide;
Neoantigen;
Cancer vaccine;
Intranodal injection;
Epitope spreading;
Tumor immunology

Abstract Probiotics are natural systems bridging synthetic biology, physical biotechnology, and immunology, initiating innate and adaptive anti-tumor immune activity. We previously constructed an all-in-one engineered food-grade probiotic *Lactococcus lactis* (FOLactis) which could boost the crosstalk among different immune cells such as dendritic cells (DCs), natural killer cells, and T cells. Herein, considering the limited clinical efficacy of naked personalized neoantigen peptide vaccines, we decorate FOLactis with tumor antigens by employing a Plug-and-Display system comprising membrane-inserted peptides. Intranodal injection of FOLactis coated with neoantigen peptides (Ag-FOLactis) induces robust DCs presentation and neoantigen-specific cellular immunity. Notably, Ag-FOLactis not only triggers a 45-fold rise in the quantity of locally reactive neoantigen-specific T cells but also induces epitope spreading in both subcutaneous and metastatic tumor-bearing models, leading to potent inhibition of tumor growth. These findings imply that Ag-FOLactis represents a powerful platform to rapidly and easily display antigens, facilitating the development of a bio-activated platform for personalized therapy.

*Corresponding authors.
E-mail addresses: liuqin@nju.edu.cn (Qin Liu), baoruiliu@nju.edu.cn (Baorui Liu).

Peer review under the responsibility of Chinese Pharmaceutical Association and Institute of Materia Medica, Chinese Academy of Medical Sciences.

https://doi.org/10.1016/j.apsb.2025.02.041

1. Introduction

Personalized neoantigen peptide-based therapeutic cancer vaccines, intended to initiate de novo T cell responses against neoantigens, are consistently regarded as safe and highly specific to tumors of individual patients. Such vaccines have the potential to enhance and diversify the endogenous repertoire of tumor-specific T cells[1]. Nevertheless, naked peptide vaccines frequently encounter substantial challenges, including premature enzymatic degradation, suboptimal antigen presentation, low immunogenicity of tumors, and restricted trafficking to lymph nodes (LNs)[2]. Current vaccine platforms typically have a singular function. Hence, there is an urgent need for an efficient tumor vaccine vector capable of swiftly presenting peptides, facilitating antigen cross-presentation, and serving as a comprehensive adjuvant all in one[3]. In contrast to nonreplicating biomaterials like Montanide ISA-51[4], mesoporous silica nanoparticles[5], and injectable hydrogels[6], live probiotics, actively involved in human health, present a promising delivery system. Through the integration of synthetic biology, chemical modification, and physical biotechnology, they can induce more robust and enduring immune responses[7,8].

Considering safety, practicality, and patient compliance, food-grade *Lactococcus lactis* possesses distinct advantages for drug delivery among probiotics, owing to its well-established and user-friendly genetic toolkit, exemplified by the Nisin Controlled Gene Expression System (NICE®)[9]. On top of it, *Lactococcus lactis* has been evaluated as a standalone treatment or in conjunction with other therapeutic approaches in various clinical trials (NCT04760353, NCT04048174, NCT04997057, NCT03751007, and NCT03893162) conducted in recent decades. Several works of literature have demonstrated the immunomodulatory impacts of *Lactococcus lactis* on natural killer cells (NKs), DCs, and macrophages by means dependent on MyD88 or NF-κB signaling pathways[10-12]. As mentioned in our previous article, we designed a multi-functional engineered *Lactococcus lactis* (FOLactis) delivering a fused protein encoding both Fms-related tyrosine kinase 3 ligand (Flt3L) and the co-stimulator OX40 ligand (OX40L)[13]. FOLactis can directly boost the localized proliferation and differentiation of a specific subset of DCs referred to as conventional type-1 DCs (cDC1), which have expertise in capturing and presenting tumor-specific antigens. Moreover, *Lactococcus lactis* can elevate the expression of OX40 on $CD4^+$ T cells, which in turn amplifies the impact of OX40L expressed by FOLactis, thereby facilitating the activation of tumor-infiltrating effector T cells (Teff) while simultaneously suppressing the function of regulatory T cells (Treg).

Tumors thrive within a dynamic microenvironment comprising malignant cells, extracellular matrix, and immune components. The collaborative action of immune cells is essential for influencing sensitivity to immunotherapy, necessitating the synchronized induction of innate and adaptive immune responses, encompassing macrophages, NKs, DCs, and T cells[14]. Recent works of literature have unveiled the significant role of NKs in recruiting DCs to tumors, consequently augmenting the elicitation of $CD8^+$ T cell responses. Additionally, IL-2 produced by T cells serves to activate NKs[15]. Likewise, DCs play a pivotal role in the efficacy of immunotherapies designed to provoke antitumor $CD8^+$ T cell responses. Upon engulfing tumor antigens, DCs especially cDC1s undergo maturation and migrate to the draining lymph nodes, where they process and present tumor antigens to $CD8^+$ T cells. Furthermore, cDC1s also play an essential role in reactivating circulating central memory T cells and facilitating their subsequent differentiation into tissue-resident memory $CD8^+$ T cells[16,17]. The evidence indicates that simultaneously activating multiple important immune cells may be one way to improve the therapeutic effect.

Tumor draining lymph nodes (TDLNs) are likely the initial site for tumor antigen presentation, but the absence of antigen or active immune suppression always contributes to the lack of immune responsiveness observed in clinically evident disease and murine models[18-20]. The appreciation for TDLNs as pivotal in the development of effective immunotherapy responses is on the rise, and it is necessary to modulate its local immune microenvironment such as augmenting the abundance of cDC1s[21]. Since systemic drug administration makes it difficult to access TDLNs, locoregional injection may bring several advantages in terms of higher local bioavailability and lower systemic toxicity[22,23]. Intranodal injection allows for the concentration of naked peptides at the tissue site where DCs and naïve T lymphocytes undergo priming, but this advantageous colocalization is transient as the afferent lymph rapidly flushes the lymph nodes[24]. Rapid vaccine degradation may compromise the quality and duration of vaccine-induced immune memory, as prolonged antigen exposure and inflammation over several days appear to optimize adaptive immune responses[25-27]. Therefore, direct immunization in TDLNs with slow-release-formulated peptides may emerge as a potentially versatile strategy to augment the efficacy of therapeutic vaccines.

In this article, we design an all-in-one genetically engineered probiotic-based personalized cancer vaccine platform (Fig. 1). Creating a universally effective tumor vaccine using a single antigen-decorated FOLactis is not practical for all patients. Thus, exploring a strategy that can swiftly and conveniently present diverse tumor neoantigens is essential for advancing personalized tumor vaccine development. We physically decorated FOLactis cell wall with neoantigen peptides by employing a cell-penetrating peptide sequence from the N-terminus of the human immunodeficiency virus Tat protein. As an engineered effective adjuvant to activate DCs, FOLactis coated with neoantigen peptides (Ag-FOLactis) can remain at the injection site, reduce the degradation of peptides, and attract DCs to capture and process vaccine antigens. In multiple subcutaneous and metastatic mouse models, locoregional injection of Ag-FOLactis in TDLNs (i.DN) markedly induces tumor-specific T cell response, augments epitope spreading, suppresses tumor growth, and extends the survival of tumor-bearing mice. Moreover, our findings indicate that Ag-FOLactis synergizes with an anti-PD1 antibody, transforming so-called "cold" non-T-cell-inflamed phenotype into "hot" inflamed tumors. In summary, we conclude that Ag-FOLactis serves as a versatile and potent personalized cancer vaccine platform for presenting various neoantigen peptides, leading to enhanced specific anti-tumor immunity with minimal harm to vital organs.

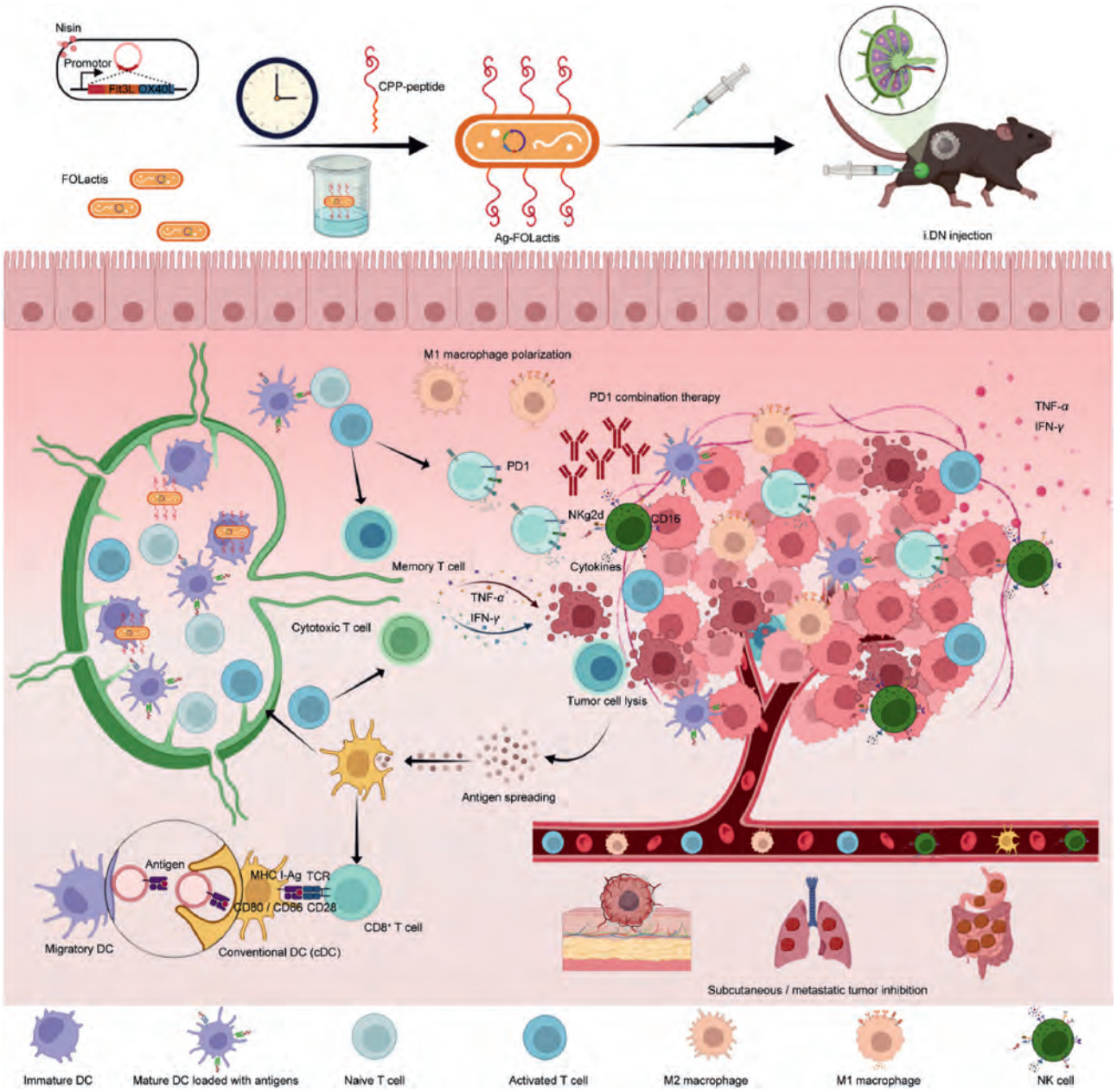

Figure 1 Schematic diagram of genetically engineered FOLactis-based personalized cancer vaccine. The engineered FOLactis was generated through transformation with a plasmid producing a fused protein of Fms-like tyrosine kinase 3 ligand and the co-stimulator OX40 ligand. Tumor neoantigen peptides were rapidly attached to the surface of FOLactis (Ag-FOLactis) with a cell-penetrating peptide (CPP) sequence. Ag-FOLactis were injected locally in the TDLNs, subsequently inducing the activation of DCs, NKs, and macrophages, resulting in the mass generation of antigen-specific T cells. In particular, sufficient tumor neoantigens could be released after tumor cell death, which endowed epitope spreading to overcome immune escape and maintain long-term anti-tumor immune responses. In multiple subcutaneous and metastatic tumor-bearing mouse models, Ag-FOLactis markedly impeded tumor growth.

2. Materials and methods

2.1. Study design

The main objective of this study is to design an all-in-one engineered probiotic-based personalized cancer vaccine platform (Ag-FOLactis). Ag-FOLactis incorporates various immune-activating functions into one, which enhances the activation of DCs, NKs, and macrophages, resulting in the mass generation of antigen-specific T cells. First, we used the NICE® system to construct FOLactis. Ag-FOLactis were characterized *in vitro* using flow cytometry (Beckman Coulter, Inc., CytoFLEX S Flow Cytometer, CA, USA), confocal microscopy (Leica Microsystems, Leica TCS SP8, Wetzlar, Germany), Western blot (Bio-Rad Laboratories, Mini-ProteanTetra, CA, USA), high performance liquid chromatography (HPLC) (Shimadzu Corporation, LC-20A Prominence, SHIMADZU, Japan), Brookhaven 90 Plus zeta Potential Analyzer (Brookhaven Instruments Co., NY, USA) and transmission

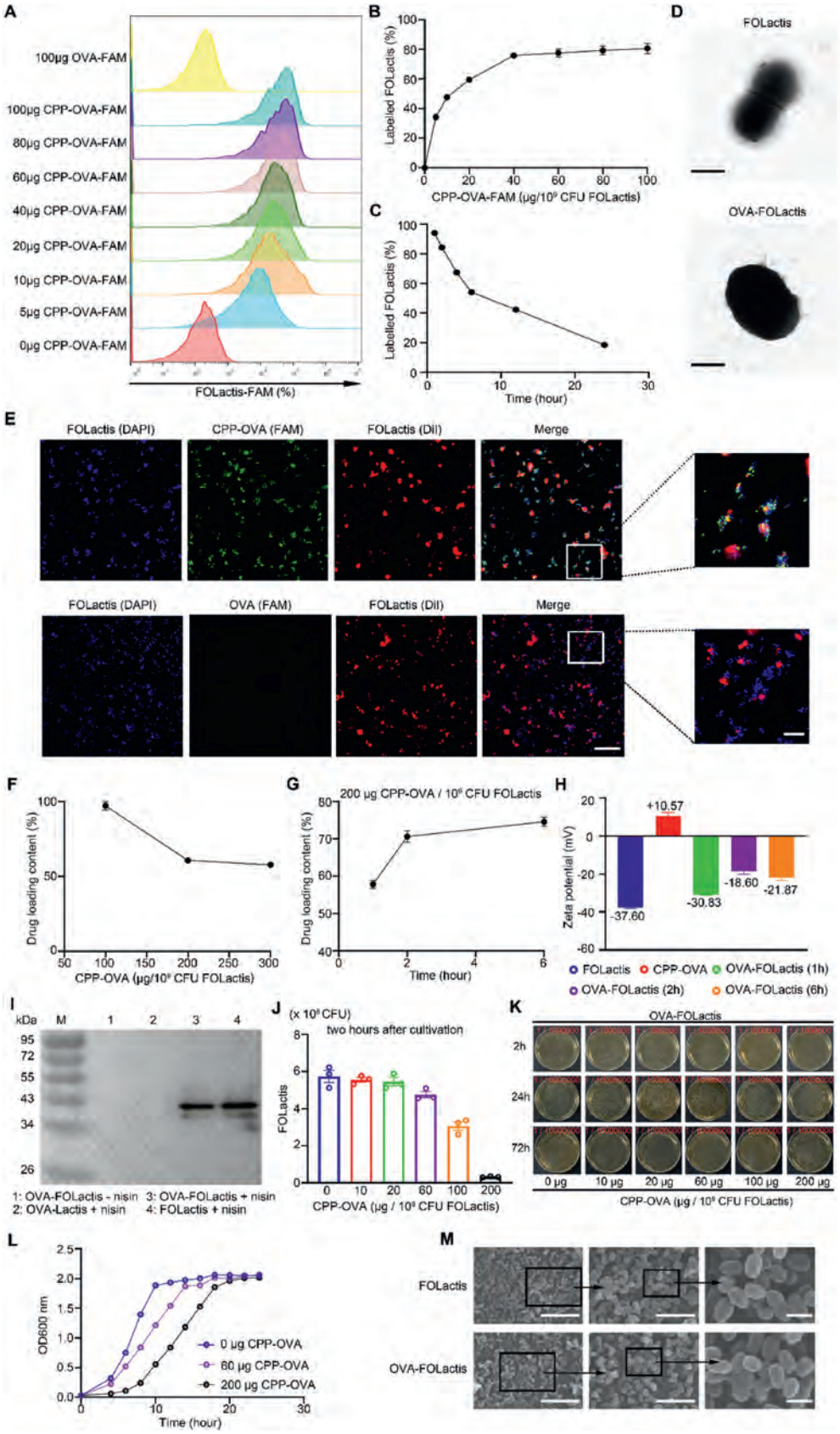

Figure 2 Display of neoantigen peptides on the FOLactis surface *via* cell-penetrating peptide sequence as an anchor. (A) Flow cytometry histograms of FOLactis coated with different amounts of CPP-OVA-FAM or OVA-FAM. (B) Assessment of the proportion of CPP-OVA-FAM modified FOLactis through flow cytometry ($n = 4$). (C) Flow cytometric examination of variations in the percentage of FOLactis coated with

electron microscopy (TEM) (FEI Company, FEI Tecnai G2 Spirit 120 KV, OR, USA). Primary murine T cells were obtained from healthy C57BL/6 mice as indicated. The abundance of antigen-specific T lymphocytes was assessed employing Elispot assay (Dakewe Biotech Co., Ltd., Mouse ELISPOT Accessory kit, Cat#: 2210006/2210007, Shenzhen, China). The antitumor effect of the Ag-FOLactis platform *in vivo* was assessed in B16F10-OVA subcutaneous melanoma and lung melanoma metastasis mouse models, as well as in MFC subcutaneous and peritoneal metastasis mouse models. We injected Ag-FOLactis locally in TDLNs and tracked tumor volume every 3−4 days post tumor engraftment using caliper measurements. Biodistribution assessment, immune profiling by flow cytometry (Beckman Coulter), and immunohistochemistry were used to characterize the system *in vivo*. Mouse body weight was monitored as a proxy for mouse health, and mice were euthanized when tumor volumes reached 1500 mm^3. Sample size is shown in the legends of each figure and all the processing has been performed in a blinded manner. All data presented in this study are indicative of a minimum of three independent replicates.

2.2. Reagents, bacterial strains, cell lines, and mice

FOLactis and FOLactis-sfGFP were designed and produced as previously described[13]. B16F10, CT26, MFC, and MC38 cells were procured from the Cell Bank of Shanghai Institute of Biochemistry and Cell Biology (Shanghai, China). All tumor cells were cultured in RPMI 1640 (Gibco, #61870036, CA, USA) supplemented with 10% fetal calf serum (Gibco, #16170078, CA, USA), 100 U/mL penicillin, and 100 μg/mL streptomycins (Meilunbio Co., Ltd., #MA0110, Dalian, China) at 37 °C and 5% CO_2. Cells were screened for Mycoplasma, and only those verified as Mycoplasma-free were utilized. Male or female 615 and C57BL/6 strains aged 5−6 weeks were procured from Shanghai Sippr-BK Laboratory Animal Co., Ltd. (Shanghai, China) and raised at the Specific Pathogen-Free (SPF) Experimental Animal Center of Affiliated Nanjing Drum Tower Hospital of Nanjing University Medical School. The facility maintained controlled conditions of temperature (68−79 °F), humidity (30%−70%), and a light/dark cycle (lights between 6 am and 6 pm). Feed and water were available ad libitum. All animal experiment protocols were approved by the Experimental Animal Care and Use Committee of Affiliated Nanjing Drum Tower Hospital of Nanjing University Medical School (2021AE01066).

2.3. Peptides

The peptides utilized in this study were as follows: SIINFEKL ($OVA_{257-264}$), SIINFEKL-FAM, GRKKRRQRRRPQRWEKISIINFEKL, GRKKRRQRRRPQRWEKISIINFEKL-FAM, GRKKRRQRRRPQRWEKISIINFEKL-CY5, DEIVMFTLI, MELLGHGMV, VENVAWTHI, LEMNFYWSL, IEFIRKFAV, LEMNFYWSLV, MELTCSSTYV, YVENVAWTHI, IDEIVMFTLI, GRKKRRQRRRPQRWEKIDEIVMFTLI, GRKKRRQRRRPQRWEKIMELLGHGMV, GRKKRRQRRRPQRWEKIVENVAWTHI, GRKKRRQRRRPQRWEKILEMNFYWSL, GRKKRRQRRRPQRWEKIIEFIRKFAV, GRKKRRQRRRPQRWEKILEMNFYWSLV, GRKKRRQRRRPQRWEKIMELTCSSTYV, GRKKRRQRRRPQRWEKIYVENVAWTHI, and GRKKRRQRRRPQRWEKIIDEIVMFTLI. The selected MFC peptides were predicted and validated as previously described[28]. Bankpeptide Biotechnology (Hefei, China) synthesized all peptides.

2.4. Preparation and characterization of Ag-FOLactis

FOLactis, reconstituted in normal saline (NS), was combined with CPP-peptides, reconstituted in NS or dimethyl sulfoxide (DMSO), and incubated for 2 h at room temperature (RT). Following complexation, Ag-FOLactis complexes were pelleted through centrifugation at 10,000×*g* for 10 min (Beckman Coulter, Inc., Microfuge 20R, CA, USA) at RT, repeating the process at least three times to eliminate unbound peptides. The zeta potential of peptides/FOLactis/Ag-FOLactis was assessed by a particle-size potentiometer (Brookhaven Instruments Co., NY, USA). We examined the dimensions and structure of Ag-FOLactis through transmission electron microscopy (FEI Company, FEI Tecnai G2 Spirit 120 KV, OR, USA) with negative staining. The morphology of Ag-FOLactis was also visualized using laser scanning confocal microscopy (Leica Microsystems). The drug loading content of Ag-FOLactis was assessed using HPLC (Shimadzu Corporation). The detection parameters for each peptide were configured based on the HPLC report as the manufacturing company supplied, including column temperature (25 °C), injection quantity (25 μL), flow rate (0.5 mL/min), and mobile phase ratio (1/1000 TFA Acetonitrile: 1/1000 TFA water = 15:85−45:55 over 13 min). The standard curve was constructed by measuring the peak areas of the free peptide at different concentrations (500, 250, 125, 62.5, and 31.25 μg/mL). The drug loading content can be determined as shown in Eq. (1):

100 μg CPP-OVA-FAM over the culture periods ($n = 6$). (D) Representative TEM images of FOLactis and FOLactis coated with 100 μg CPP-OVA. Black scale bars: 0.5 μm. (E) Confocal images of FOLactis coated with 100 μg CPP-OVA or OVA peptides. FOLactis were stained with blue (DAPI) or red (DiI) and CPP-OVA or OVA peptides were stained with green (FAM), respectively. White scale bars: 50 μm (Left), 10 μm (Right). (F) Drug loading content of different concentrations of CPP-OVA peptide determined by high-performance liquid chromatography (HPLC) ($n = 3$). (G) Drug loading content of 200 μg CPP-OVA peptide determined by HPLC at different times of co-incubation with 10^9 CFU FOLactis ($n = 3$). (H) Zeta potential ($n = 3$) of FOLactis, CPP-OVA, FOLactis incubated with 200 μg CPP-OVA for 1 h, FOLactis incubated with 200 μg CPP-OVA for 2 h and FOLactis incubated with 200 μg CPP-OVA for 6 h. (I) Western blotting analysis of the induced or non-induced OVA-FOLactis. Nisin is an inducer of protein expression. M: molecular mass marker; The lanes (1−4) represent the whole bacterial lysates (bacteria) of non-induced OVA-FOLactis, OVA-Lactis induced by nisin, OVA-FOLactis induced by nisin, and FOLactis induced by nisin, respectively. OVA-FOLactis, FOLactis coated with 100 μg CPP-OVA-FAM. OVA-Lactis, wild-type *Lactococcus lactis* coated with 100 μg CPP-OVA-FAM. (J−K) Quantification (J) of bacterial colonization and representative photographs of solid GM17 agar plates (K) at the indicated time points after FOLactis co-incubated with different amounts of CPP-OVA peptides (OVA-FOLactis) for 2 h in normal saline (NS) at room temperature. (L) The growth trajectories of uncoated and coated FOLactis were assessed by culturing bacteria in GM17 medium at 30 °C, and we recorded the optical density at 600 nm (OD600) at specified time intervals. (M) Scanning electron microscope images of FOLactis and FOLactis coated with 200 μg CPP-OVA peptide after they were cultured at 30 °C in liquid GM17 medium without agitation for 24 h. White scale bars: 10 μm (Left), 5 μm (Middle), 1 μm (Right). Data were mean ± SEM.

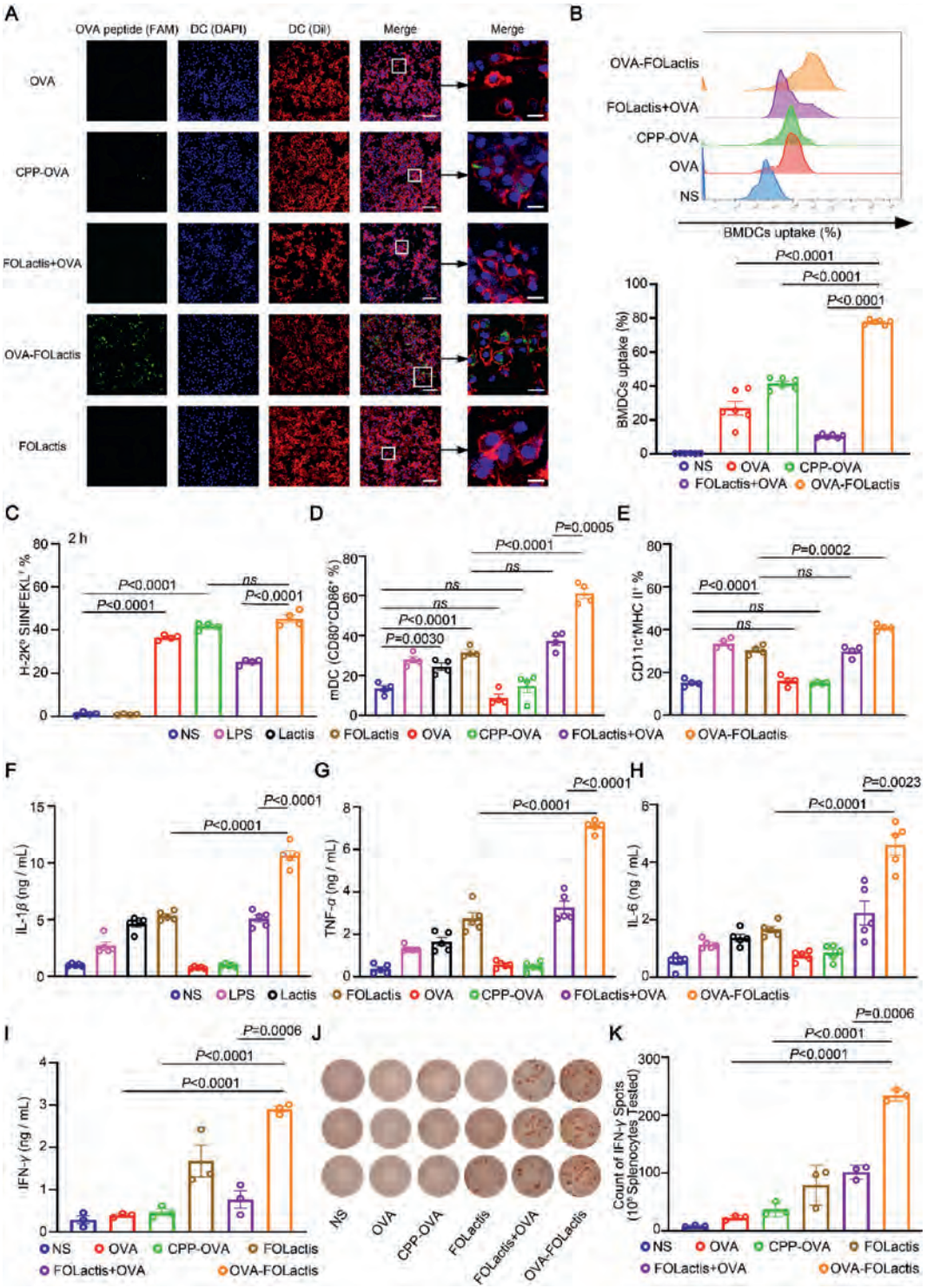

Figure 3 Neoantigen peptides delivered by FOLactis can be efficiently presented by DCs and induce antigen-specific T-cell responses. (A) Colocalization analysis of OVA, CPP-OVA, FOLactis + OVA, OVA-FOLactis (OVA-FAM/CPP-OVA-FAM, green), and FOLactis in Dil-labeled DCs (red) using confocal microscopy after a 2-h incubation. BMDCs, bone marrow-derived DCs. White scale bars: 100 μm (Left), 20 μm (Right). (B) Cellular uptake of OVA, CPP-OVA, FOLactis + OVA, and OVA-FOLactis (OVA-FAM/CPP-OVA-FAM; green) after a 2-h incubation with BMDCs, as determined by flow cytometry (n = 6). (C) BMDCs were pulsed with FOLactis, OVA, CPP-OVA, FOLactis + OVA, and OVA-FOLactis for 2 h. Flow cytometry was employed to evaluate cross-presentation, utilizing PE-conjugated anti-H-2Kb antibodies bound to SIINFEKL. (D) The percentage of $CD80^+CD86^+$ DCs after co-incubation with LPS, Lactis, FOLactis, OVA, CPP-OVA, FOLactis + OVA or OVA-FOLactis *in vitro* for 24 h (n = 4). (E) Flow cytometry analysis of MHC II^+ BMDCs after incubation with LPS, FOLactis, OVA, CPP-OVA, FOLactis + OVA, or OVA-FOLactis for 24 h (n = 4). (F–H) Concentrations of pro-inflammatory cytokines in BMDC supernatants were measured after a 24-h incubation with LPS, Lactis, FOLactis, OVA, CPP-OVA, FOLactis + OVA, or OVA-FOLactis (n = 5). (I) The

Drug loading content (%) = Weight of the peptides coated on FOLactis / Weight of the total peptides × 100 (1)

2.5. In vitro T-cell activation

We obtained Bone Marrow Derived Cells (BMDCs) from bone mesenchymal stem cells harvested from C57BL/6 mice freshly. Then the cells were cultured with RPMI 1640 medium (Gibco) containing 10% FBS (Gibco) and 1% penicillin−streptomycin (Meilunbio Co., Ltd.). We added 20 ng/mL rmGM-CSF (Xiamen Amoytop Biotech Co., Ltd., IMF-GMF, Xianmen, China) and 10 ng/mL rmIL-4 (PeproTech, 214-14, NJ, USA) to the medium to induce the cells to differentiate into DCs. The medium was replaced every three days and these DCs were centrifuged at 300×*g* for 5 min (Beijing Baiyang Medical Instruments Co., Ltd., BY-300C, Beijing, China), and collected for use on Day 8. Lymphocytes were isolated from splenocytes of C57BL/6 mice and co-incubated with DCs at the ratio of 10: 1, which were then co-cultured with NS, 10 nmol OVA peptides, 10 nmol CPP-OVA peptides, 1.5×10^8 CFU FOLactis, 1.5×10^8 CFU FOLactis + 10 nmol OVA peptides, or 1.5×10^8 CFU FOLactis decorated with 10 nmol CPP-OVA peptides respectively for 24 h. Finally, the cells were collected by centrifugation at 300×*g* for 5 min (Beijing Baiyang Medical Instruments Co., Ltd., BY-300C, Beijing, China) and assessed by flow cytometry analysis (CytExpert 2.4).

2.6. Immunization and tumor therapy experiments

For subcutaneous melanoma and lung melanoma metastasis mouse models, C57BL/6 mice were inoculated with 2×10^5 B16F10-OVA cells subcutaneously or intravenously. We injected NS, 20 nmol CPP-OVA, 10^9 CFU FOLactis, and OVA-FOLactis (10^9 CFU FOLactis coated with 20 nmol CPP-OVA) locally in the LNs on Days 3, 5, 7, 9 and 11. We dissolved all the drugs in 50 μL NS. In the mouse models of MFC subcutaneous and peritoneal metastasis, 5×10^5 tumor cells were administered either subcutaneously (s.c.) or intraperitoneally (i.p.). MFC tumor-bearing mice were immunized by i.DN injection of different drugs including NS, nine mutant antigens from MFC cells (MFC_{mix}, 10 nmol each peptide), 2×10^9 CFU FOLactis, and MFC_{mix}-FOLactis (2×10^9 CFU FOLactis coated with MFC_{mix}) on the indicated days. Intralymph node injections were performed by injecting tracer dye subcutaneously into the dorsal toe of mice, then injecting vaccines i.DN after tracer drainage as previously described[29,30].

The volume of tumors (V, mm^3) was assessed every 2−3 days as shown in Eq. (2):

$$V = (\text{Width})^2 \times \text{Length} \times 0.5 \quad (2)$$

The maximum allowable tumor burden was set at 1500 mm^3. In certain instances, this limit was surpassed on the final day of measurement, leading to the immediate euthanization of the mice. Central organs, encompassing the hearts, livers, spleens, lungs, and kidneys, were gathered, and subjected to hematoxylin−eosin (H&E) staining utilizing optical microscopy (Thermo Fisher Scientific, Thermo Fisher Invitrogen™ EVOS™ M7000, MA, USA). On Day 18, mice with lung melanoma metastasis were euthanized. Following a 48-h fixation with 4% paraformaldehyde, lung photographs were captured, and the enumeration of pulmonary tumor nodules was performed. Blood was obtained from the mice *via* enucleation and subsequently centrifuged (3000 rpm, 10 min, Beckman Coulter, Inc., Microfuge 20R, CA, USA) to isolate the serum. The LEGENDplex™ MU Th1/Th2 Panel (8-plex) w/VbP V03 (Biolegend, # 741054, CA, USA) was employed to assess the concentration of the eight factors (IFN-γ, TNF-α, IL-5, IL-13, IL-2, IL-6, IL-10, IL-4).

To test the combination therapy of Ag-FOLactis and anti-PD1 (100 μg per mouse), we randomly divided B16F10-OVA tumor-bearing mice into four groups including NS, PD1, OVA-FOLactis, and OVA-FOLactis + PD1. Intraperitoneal (i.p.) injections of anti-PD1 were administered on Days 5, 7, and 9.

To analyze specific tumor killing, we isolated splenocytes from mice to perform intracellular IFN-γ staining and IFN-γ Elispot analysis (Dakewe) as the manufacturer instructed. In brief, we stained CD3 and CD8 on the surface of splenocytes before IFN-γ staining. Subsequently, we fixed the cells using BD Cytofix/Cytoperm™ Fixation and Permeabilization Solution (Becton, Dickinson and Company, #554722, NJ, USA), followed by permeabilization. The permeabilized cells were then washed with BD Perm/Wash™ Perm/Wash Buffer (Becton, Dickinson and Company, #554723, NJ, USA) and suspended in cell staining buffer for flow cytometry analysis using the Beckman CytoFlex. In the IFN-γ Elispot assays, splenocytes were seeded at a density of 1×10^5 cells per well in a 96-well plate that had been precoated with a mouse anti-IFN-γ antibody. The cells were then incubated with peptide antigen for 18−20 h ($n = 3$). The detection process followed the guidelines outlined in the mouse IFN-γ ELISPOT kit manual provided by Dakewe in China. Briefly, after cell lysis and plate washing, we added the detection antibody IFN-γ (diluted at 1:100 with 100 μL per well) to the plates. Incubated the plates at 37 °C for 1 h. After another round of plate washing, we introduced the diluted streptavidin-HRP (also at a 1:100 dilution, with 100 μL per well) and incubated the plates for another hour. Subsequently, we treated the wells with a mixture of 3-amino-9-ethylcarbazole (AEC) solution and placed the plates in a dark room at RT. The development process was monitored at 5-min intervals, and the reaction was halted by adding deionized water. We scanned plates with ELISPOT CTL Reader (Cellular Technology Inc., USA) and analyzed the results with Elispot software (AID Diagnostika GmbH, Germany).

2.7. BMDCs uptake of OVA-FOLactis-FAM in vitro

Mesenchymal stem cells from the bone marrow were extracted from the femur and tibia of C57BL/6 mice. To induce cell differentiation into DCs, we supplemented the medium with 20 ng/mL rmGM-CSF (Xiamen Amoytop Biotech Co., Ltd.) and 10 ng/mL rmIL-4 (PeproTech). On Day 8, the immature DCs collected were suspended in a complete medium without cytokines and

concentration of IFN-γ secreted by splenocytes of C57BL/6 mice stimulated by OVA, CPP-OVA, FOLactis, FOLactis + OVA or OVA-FOLactis ($n = 3$, biologically independent samples). (J−K) IFN-γ secretion, assessed through the ELISPOT assay, from splenocytes that underwent re-stimulation with $OVA_{257-264}$ (J) ($n = 3$). The quantitative analysis of IFN-γ secretion in the ELISPOT assay is depicted in (K) ($n = 3$). OVA-FOLactis, 1.5×10^8 CFU FOLactis coated with 10 nmol CPP-OVA-FAM/CPP-OVA peptides. The data (B−I, K) were shown as mean ± SEM. Statistical analysis was performed by two-tailed unpaired Student's *t*-test. *ns* represented $P > 0.05$.

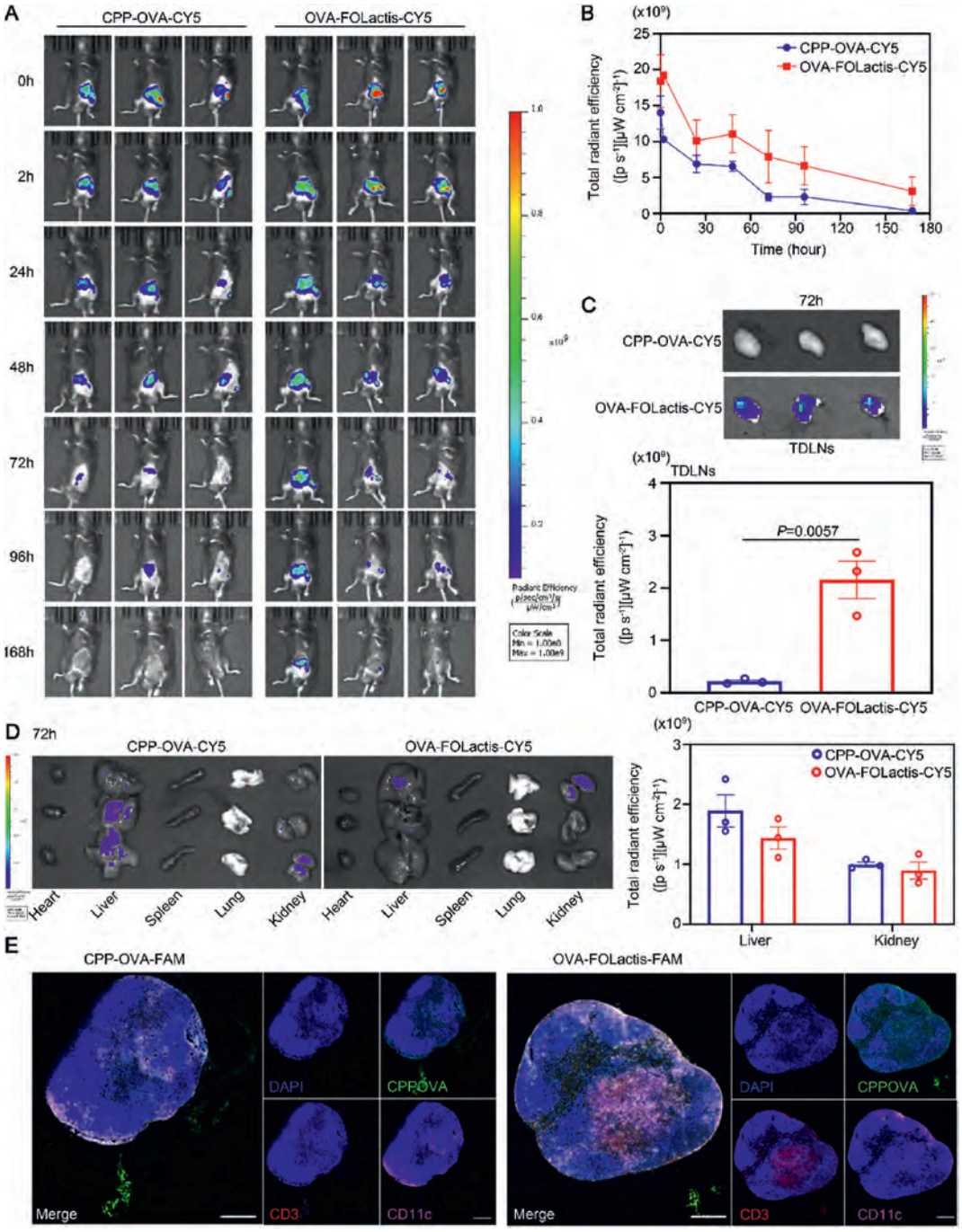

Figure 4 Biodistribution analysis of neoantigen peptides in lymph nodes through locoregional administration. (A) Equivalent peptide-CY5 (CPP-OVA-CY5 group) and FOLactis-peptide-CY5 (OVA-FOLactis-CY5 group) were injected locally in tumor draining lymph nodes (TDLNs). Near-infrared (NIR) imaging captured the fluorescence distribution *in vivo* at various time intervals ($n = 3$). (B) The overall radiant efficiency of peptide signal in mice over time ($n = 3$). (C) The overall radiant efficiency of peptides signals in TDLNs *ex vivo* throughout the observation period ($n = 3$). (D) Total radiant efficiency of spleens and kidneys 72 h after injection. (E) Immunofluorescence staining of $CD3^+$ cells, $CD11c^+$ cells, and peptides in TDLNs of mice in CPP-OVA-FAM and OVA-FOLactis-OVA groups. White scale bars, 400 μm. In experiments B−D, the error bars represented mean ± SEM, and statistical significance was determined by two-tailed unpaired Student's *t*-test.

co-cultured with the specified drugs for 24 h. Ultimately, all cells were gathered through centrifugation at 300×*g* for 5 min (Beijing Baiyang Medical Instruments Co., Ltd., BY-300C, Beijing, China) and subsequently incubated with 1 μL of the corresponding monoclonal antibody for 30 min before undergoing flow cytometry testing. The cytokines in the supernatant were tested as instructions.

In the cross-presentation assay, OVA-FOLactis-FAM was co-incubated with DiI-stained-DCs for 2 h, and the cells were visualized using a confocal laser scanning microscope (Leica).

We harvested C57BL/6 mouse-derived splenocytes for T-cell testing. Add them to 96-well plates at 1×10^6 cells/mL in 100 μL AIMV medium (Gibco, #0870112DK, CA, USA) containing 10%

FBS (Gibco). Then we incubated 1×10^5 splenocytes with NS, OVA, CPP-OVA, FOLactis, FOLactis + OVA, and OVA-FOLactis on Day 0, and stimulated again on Day 3. Remove all supernatants on Day 6, and add OVA peptides to the corresponding cells in a 96-well plate to co-culture for 24 h. The supernatant was gathered and analyzed using BD™ Cytometric Bead Array (CBA) Mouse IFN-γ Flex Set (Becton, Dickinson and Company, #558296, NJ, USA). The method for determining the frequency of IFN-γ-secreting T cells is identical to the one described above, and the detection was conducted following the instructions in the mouse IFN-γ ELISPOT kit manual (Dakewe).

2.8. Near-infrared imaging of mice

Equivalent peptide-CY5 and FOLactis-peptide-CY5 were separately injected locally in the TDLNs. Mice were anesthetized with isoflurane and scanned at indicated time points, respectively employing a CRi Maestro *In Vivo* Imaging System (Cambridge Research & Instrumentation, MA, USA). Subsequently, mice were euthanized, and inguinal lymph nodes, hearts, livers, spleens, lungs, and kidneys were extracted and imaged. Image analysis involved the use of ROI to define specific areas for calculating the average fluorescence intensity.

2.9. Immunofluorescence staining

TDLNs were obtained 72 h post-treatment, processed into frozen sections, and subjected to overnight incubation with anti-CD3 rabbit monoclonal antibody (1:200) (Abcam, #ab237721, Cambridge, UK), anti-CD8 rabbit monoclonal antibody (1:200) (Abcam, #ab217344, Cambridge, UK), and anti-CD11c Rabbit mAb (1:200) (Cell Signaling Technology, #97585, Boston, USA) at 4 °C. Following three washes with PBS, the sections were stained with goat anti-rabbit IgG H&L (Abcam, Alexa Fluor® 555, #ab150078, Cambridge, UK), goat anti-rabbit IgG H&L (Abcam, Alexa Fluor® 594, #ab150080, Cambridge, UK), and DAPI (Sangon Biotech (Shanghai) Co., Ltd, #E607303, Shanghai, China). The sections were then sealed with 50% glycerol, and fluorescence images were captured using a confocal microscope (Leica).

2.10. Tumor cell killing assay

The splenocytes obtained from the immunized mice were used for tumor-killing assay. To label the tumor cells, we incorporated 1 μmol/L CFSE (Sangon Biotech (Shanghai) Co., Ltd., #A447100, Shanghai, China) into 1×10^6/mL tumor cells and incubated them at 37 °C in darkness for 8−10 min. Subsequently, we introduced a volume of RPMI 1640 (Gibco) supplemented with 10% FBS (Gibco) that was ten times greater to halt the labeling reaction. After centrifuging at $300 \times g$ for 5 min (Beijing Baiyang Medical Instruments Co., Ltd., BY-300C, Beijing, China), discard the supernatant to obtain the tumor cells as target cells. Splenocytes served as effector cells and were incubated with target cells at effector-to-target ratios of 5:1, 10:1, and 20:1, respectively, at 37 °C for the specified duration. We added 50 ng/mL PI solution (Sangon Biotech (Shanghai) Co., Ltd., #A425259, Shanghai, China) into the collected cells, incubated them at RT in the dark for 10 min, and conducted the analysis by BeckMan CytoFlex.

2.11. Flow cytometry

Antibodies to CD11c (N418, FITC, 117306), CD80 (16-10A1, APC, 104714), CD86 (GL-1, PE, 105008), MHC II (M5/114.15.2, APC, 107614), H-2K^b bound to SIINFEKL (25-D1.16, PE, 141604), CD3 (17A2, FITC, 100204), CD8a (53-6.7, APC, 100712), CD44 (IM7, PE, 103008), CD62L (MEL-14, PE/Cyanine7, 104418), CD8a (53-6.7, PerCP/Cyanine5.5, 100734), CD69 (H1.2F3, FITC, 104506), IFN-γ (XMG1.2, APC, 505810), CD103 (2E7, PE, 121406), CD4 (GK1.5, PE/Cyanine7, 100422), CD25 (PC61, APC, 102012), FoxP3 (MF-14, PE, 126404), NK 1.1 (PK136, PE, 108708), CD 11b (M1/70, FITC, 101206), F4/80 (BM8, PE/Cyanine5, 123112), CD206 (C068C2, PE, 141706), PD1 (29F.1A12, APC, 135210), PD-L1 (MIH7, PE, 155404) were purchased from Biolegend.

The minced tumor tissue underwent digestion with collagenase type IV (Sigma−Aldrich, #C4-BIOC, MO, USA) at 37 °C for 2 h under gentle agitation. Mechanical grinding was employed to generate single-cell suspensions from TDLNs and spleens. All cell samples were suspended in NS and stained with the appropriate flow cytometry antibodies for 30 min. After two washes, we conducted flow cytometry analysis using Beckman CytoFlex.

2.12. Transcriptome sequencing (RNA-seq)

RNA-seq analysis of mouse tumor tissues was conducted by Berry Genomic Company (Beijing, China). Differential gene analysis between the NS and the OVA-FOLactis group was performed using the DESeq2 Bioconductor package. We performed an analysis of functionally related Gene Ontology (GO) terms for biological processes using GOSeq (v1.34.1). For the Kyoto Encyclopedia of Genes and Genomes (KEGG) enrichment analysis, we utilized the database available at http://en.wikipedia.org/wiki/KEGG as a reference. GO network analysis of significantly up and downregulated genes in tumors was analyzed by Cytoscape software. All data were analyzed using the R software (version 3.6.3) and GraphPad Prism 8 (San Diego, CA, USA).

2.13. Statistical analysis

In all experiments, unless specified otherwise, we conducted at least three independent biological replicates. Statistical analyses and graph plotting were carried out employing GraphPad Prism 8.0.2 (San Diego, CA, USA). All results were presented as means ± standard error of mean (SEM). For tumor burden comparisons, p-values were calculated by two-tailed unpaired Student's *t*-test or two-way ANOVA and Tukey post-test and correction as indicated. For survival studies, log-rank (Mantel-Cox) tests were used. For flow cytometry studies and other experiments, student's *t*-test were used. Flow cytometry data were obtained using a Beckman CytoFlex instrument (USA) and assessed using FlowJo software. Figures were created using Adobe Photoshop.

3. Results

3.1. Display of neoantigen peptides on the FOLactis surface via a cell-penetrating peptide sequence as an anchor

The cell wall of *Lactococcus lactis* comprises a highly intricate structure that includes various lipid components[31], which might be attached into by therapeutic neoantigen peptide sequences anchored with a cell-penetrating peptide (CPP). Thus, we opted for a CPP sequence derived from HIV Tat protein and conjugated it to the N-terminus of the therapeutic neoantigen peptides. For a more in-depth examination of binding affinities and the amount of

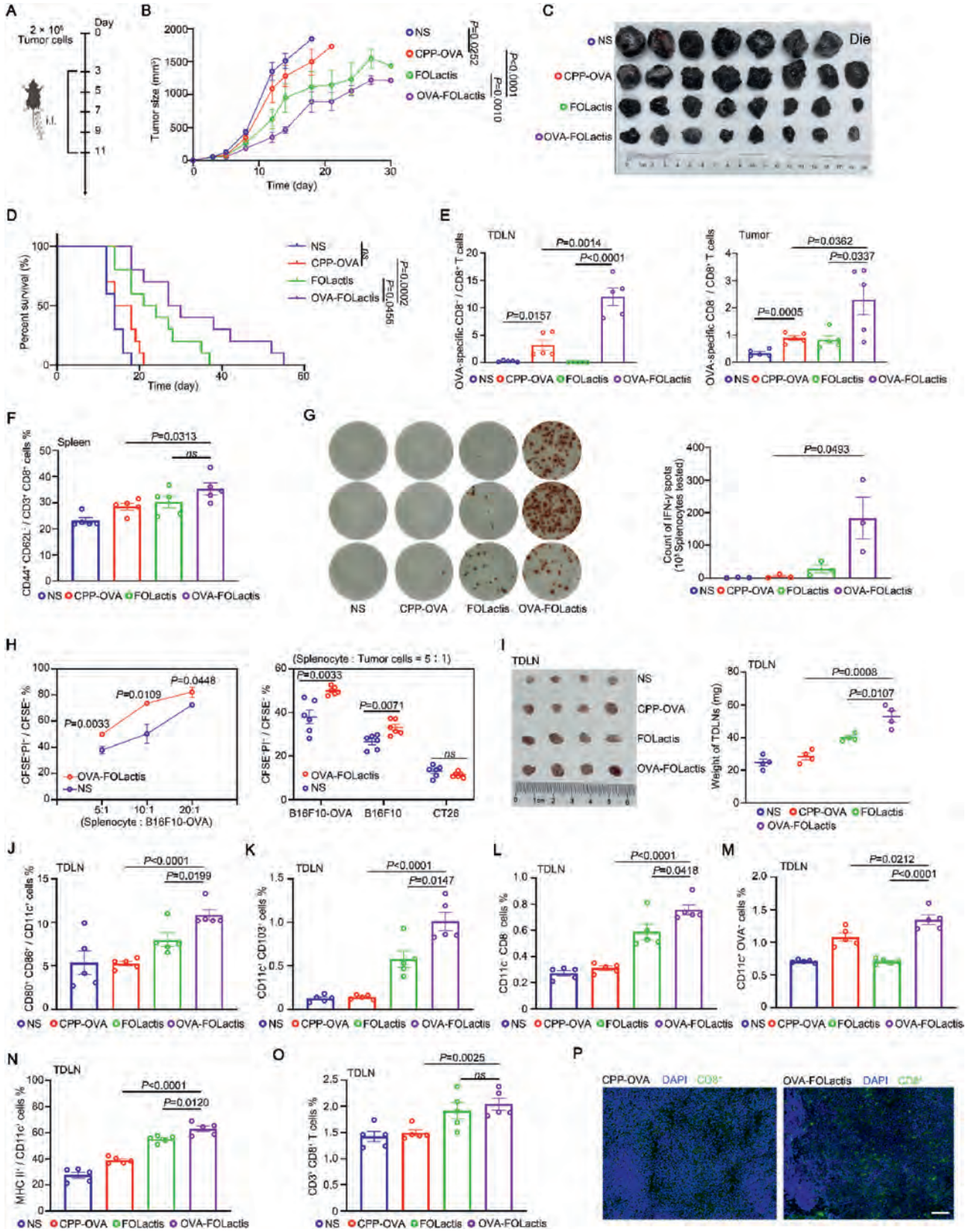

Figure 5 Antitumor activity of single antigen ($OVA_{257-264}$) displayed by FOLactis. (A) Illustration outlining the B16F10-OVA subcutaneous tumor model. Mice were inoculated with 2×10^5 B16F10-OVA melanoma cells on Day 0. When the tumor size reached nearly 50 mm^3, the mice received immunizations with the following vaccines: normal saline (NS); 20 nmol CPP-OVA peptides; 10^9 CFU FOLactis; or 10^9 FOLactis coated with 20 nmol CPP-OVA peptides (OVA-FOLactis) for five times. Tumor size was assessed every 2−3 days. Immune responses were analyzed on

peptides bound to FOLactis, we incubated 10^9 CFU FOLactis with different amounts of CPP-OVA-FAM peptides. The CPP-OVA-FAM peptides were shown to spontaneously transfer from solution to the FOLactis surface after co-culturing for 1 h at RT (Fig. 2A). Almost 60 μg CPP-OVA-FAM created an 80% coating of 10^9 CFU FOLactis (Fig. 2B). Given that binding stability is a crucial parameter for surface modification, we cultured FOLactis coated with 100 μg CPP-OVA-FAM (OVA-FOLactis-FAM) in liquid GM17 medium at 30 °C without shaking and found that the percentage of OVA-FOLactis-FAM declined to 50% after culturing for 6 h, when the number of FOLactis approximately doubled (Fig. 2C). On top of that, it was shown that the percentage of OVA-FOLactis-FAM remained stable if they were cultured in normal saline (NS) at 4 °C for at least two weeks (Supporting Information Fig. S1). We characterized the morphology of FOLactis using TEM (FEI Company). In contrast to the smooth and transparent uncoated FOLactis, FOLactis coated with 100 μg CPP-OVA displayed rough and opaque edges (Fig. 2D). Confocal laser scanning microscopy (Leica Microsystems) also revealed fluorescent CPP-OVA peptide localized on FOLactis successfully, indicating that the CPP sequence is the key to anchoring bacteria (Fig. 2E). In order to clarify the modification conditions of decorating FOLactis with peptides in more detail, we determined the drug loading content using high HPLC (Shimadzu Corporation). When co-incubated for 1 h at RT, 10^9 CFU FOLactis can carry about 100 μg CPP-OVA (Fig. 2F). With the increase of peptide content and the extension of time, the drug loading content of CPP-OVA has increased (Fig. 2G). The results suggested that the drug loading content of CPP-OVA could be affected by total peptide content and co-incubation time. The average zeta potentials of 10^9 CFU FOLactis incubated with 200 μg CPP-OVA for different times were shown as Fig. 2H. This modification strategy did not compromise the protein expressed by FOLactis (Fig. 2I).

Next, we planned to use an engineered Lactis expressing a fusion protein comprising Flt3L, OX40L, and sfGFP (FOLactis-sfGFP)[13] to examine whether the expressed heterologous protein maintained its biological structure and activity after Lactis decorated with different amounts of CPP-OVA peptides for 2 h in NS at RT. Notably, both flow cytometric analysis and fluorescence of FOLactis-sfGFP indicated that CPP-OVA peptides did no harm to the heterologous protein expressed by engineered Lactis (Supporting Information Fig. S2). In addition, we also evaluated the viability and growth of the decorated probiotic, which were crucial for the implementation of this approach. As indicated by the plate counting results presented in Fig. 2J−K, nearly 90% bacteria viability was observed when the amounts of CPP-OVA increased up to 60 μg 2 h after cultivation. FOLactis in all groups recovered 24 h after cultivation, which was similar to the record of OD600 illustrated (Fig. 2L). Furthermore, the scanning electron microscope images indicated that the structure of FOLactis coated with 200 μg CPP-OVA was unaffected compared to native FOLactis 24 h after cultivation (Fig. 2M). In conclusion, all the findings affirmed the straightforwardness and practicality of decorating FOLactis with CPP-peptides.

3.2. Neoantigen peptides delivered by FOLactis can be efficiently presented by DCs and elicit antigen-specific T-cell responses

Internalization into DCs plays a crucial role in the processing and presentation of tumor-specific antigens[32]. A successful T-cell-mediated adaptive immune response requires two main steps. One is interactions between antigen-specific T-cell receptors (TCRs) and antigenic peptides presented on major histocompatibility complex (MHC) molecules on antigen-presenting cells (APCs)[33]. The other is the activation of co-stimulatory receptor CD28 on T cells by co-stimulatory molecules CD86 and CD80 expressed on APCs[34]. Thus, we investigated the internalization of FOLactis coated with CPP-OVA by DCs, DCs maturation, and the subsequent T cell activation. Firstly, we incubated 10^6 BMDCs with 10 nmol OVA-FAM peptides, 10 nmol CPP-OVA-FAM peptides, 1.5×10^8 CFU FOLactis + 10 nmol OVA-FAM peptides, 1.5×10^8 CFU FOLactis coated with 10 nmol CPP-OVA-FAM peptides (FAM-OVA_{10nmol}-FOLactis), and 1.5×10^8 CFU FOLactis, respectively. It was shown that most, if not all, FAM-OVA_{10nmol}-FOLactis were internalized into BMDCs (Fig. 3A). We also evaluated cell-associated fluorescence through flow cytometry and found that BMDCs in the FAM-OVA_{10nmol}-FOLactis group (77.58%) exhibited about eight-fold greater fluorescence than the FOLactis + OVA-FAM group (10.47%), which may suggest that the co-delivered formulation was far more effective in antigen presentation than the mixing of the separate components (Fig. 3B). Notably, the detection of MHCI H-$2K^b$-presented $OVA_{257-264}$ (MHCI-OVA) on BMDCs indicated the similar result (Fig. 3C and Supporting Information Fig. S3A). We supposed that DCs were inclined to take up FOLactis and might be premature, which seriously restricted sufficient antigen uptake and presentation. It is critical to decorate FOLactis with

Day 18. (B) Tumor growth curves over 30 days were plotted to depict the average response to different treatments in C57BL/6 mice ($n = 8$). *P*-values were determined by two-way ANOVA with Tukey's multiple comparisons test. *ns* represented $P > 0.05$. (C) Photos of tumors harvested from mice seven days post the last treatment ($n = 8$). (D) Survival curves of C57BL/6 mice over 60 days ($n = 10$). *P*-values were calculated using log-rank (Mantel−Cox) test. *ns* represented $P > 0.05$. (E) TDLNs and Tumors were collected on Day 18, and the flow cytometric analysis of OVA tetramer$^+$ in CD8$^+$ cells ($n = 5$). (F) Analysis of immune memory on Day 18. The percentages of effector memory T cells (CD3$^+$CD8$^+$CD44$^+$CD62L$^-$) in the splenocytes ($n = 5$). (G) The Elispot assay was utilized to assess IFN-γ secretion by splenocytes after re-stimulation with OVA peptide, and quantitative analysis of the Elispot data was conducted ($n = 3$). (H) We derived splenocytes of mice in the NS or OVA-FOLactis group and incubated them with CFSE-labeled tumor cells (B16F10-OVA, B16F10, CT26) at different effector-to-target ratios. Propidium iodide was introduced 6 h after incubation, and the proportion of dead cells was examined by flow cytometry ($n = 6$). (I) The inguinal lymph nodes from mice on Day 18 were collected, photographed, and weighed ($n = 4$). (J−O) Mice from various groups were euthanized one week after the final treatment, and the proportions of immune cells in the local TDLNs were examined by flow cytometry ($n = 5$). Analysis of CD80$^+$CD86$^+$ gated on CD11c$^+$ DCs (J), CD11c$^+$CD103$^+$ cells (K), CD11c$^+$CD8$^+$ cells (L), CD11c$^+$OVA$^+$ cells (M), MHC II$^+$ DCs gated on CD11c$^+$ DCs (N), and CD3$^+$CD8$^+$ T cells (O) in the TDLNs using flow cytometry. (P) Immunofluorescence staining of CD8$^+$ cells in TDLNs of mice in CPP-OVA and OVA-FOLactis groups. White scale bar, 50 μm. For the experiments in (E−O), statistical significance was determined using analysis of two-tailed unpaired Student's *t*-test. *ns* represented $P > 0.05$.

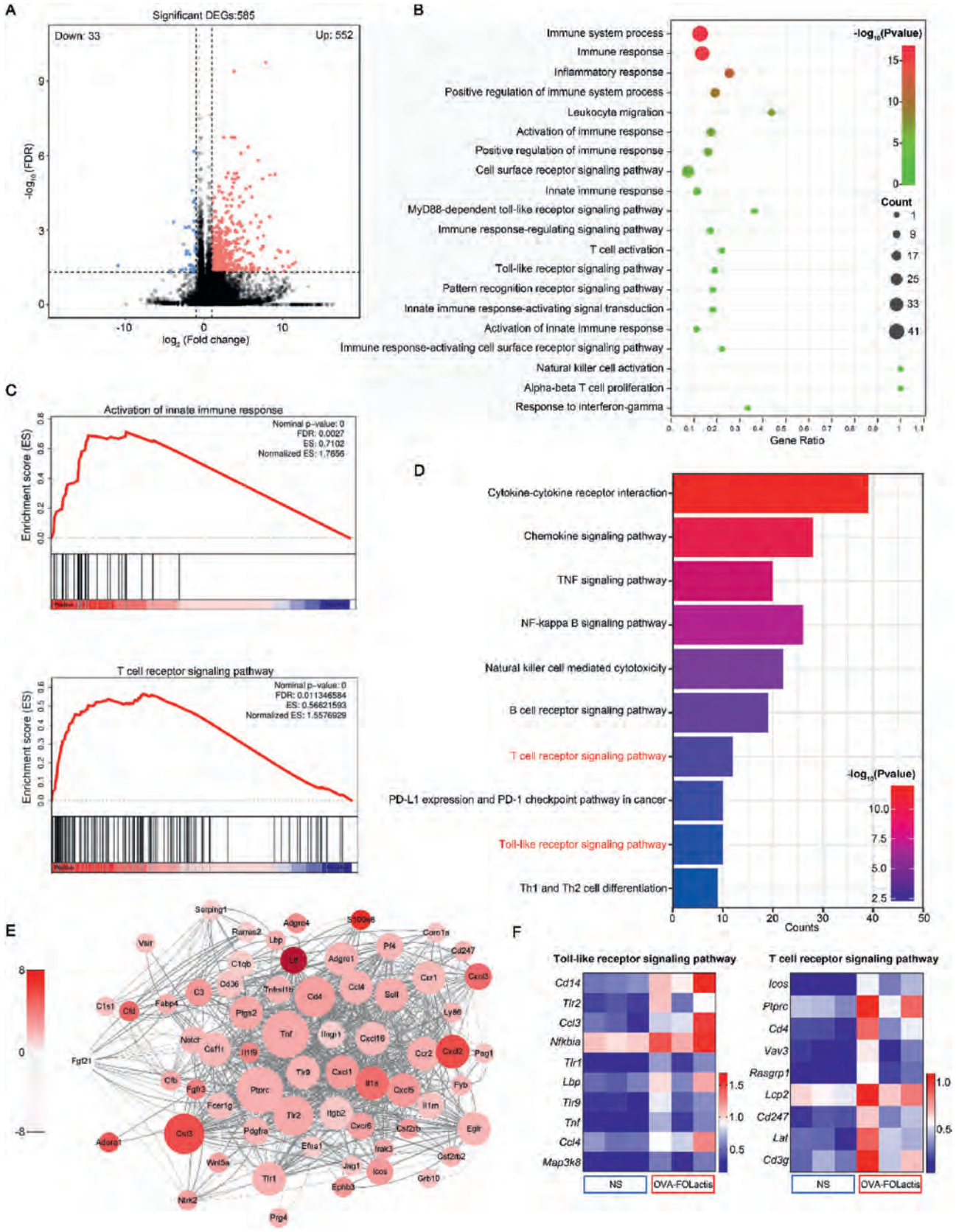

Figure 6 RNA-seq analysis of tumors after OVA-FOLactis administration. (A) Volcano map of differentially expressed genes (DEGs) between the NS and OVA-FOLactis groups ($n = 3$). (B) Gene Ontology (GO) analysis. (C) Gene Set Enrichment Analysis (GSEA) analysis. (D) Kyoto Encyclopedia of Genes and Genomes (KEGG) enrichment analysis. (E) GO network analysis of significantly up- and downregulated genes in tumors from mice in the OVA-FOLactis group, in comparison to those treated with NS. The color scales indicate log_2-transformed fold change

CPP-peptides to make them a co-delivered formulation. Since FOLactis is an effective immune adjuvant, it was shown a notable rise in the percentage of mature DCs ($CD80^+$ $CD86^+$) and MHC II^+ DCs upon culturing BMDCs with FOLactis, FOLactis + OVA and FOLactis coated with CPP-OVA (OVA_{10nmol}-FOLactis) for 24 h (Fig. 3D and E; Fig. S3B and S3C). To assess the induction of innate immune responses, the cytokine secretion in the culture medium of BMDCs was further examined. As illustrated in Fig. 3F−H, the secretion of IL-1β, TNF-α, and IL-6 exhibited a significant increase in the OVA_{10nmol}-FOLactis group.

Next, we investigated T cell activation *in vitro* using splenocytes from C57BL/6 mice. Over seven days, splenocytes were tested for IFN-γ levels after peptide pulses three times. Compared with naked OVA and CPP-OVA peptides, the concentration of IFN-γ induced by OVA_{10nmol}-FOLactis increased more than six-fold ($P < 0.0001$) (Fig. 3I). We evaluated the presence of antigen-specific T lymphocytes using the enzyme-linked immunospot (Elispot) assay (Dakewe). It was demonstrated that splenocytes immunized with OVA_{10nmol}-FOLactis exhibited increased secretion of OVA peptide-specific IFN-γ when exposed to $OVA_{257-264}$, surpassing the other groups (Fig. 3J and K). Similarly, it was shown that OVA-FOLactis significantly increased the proportion of CD25 and CD69 expression on T cells compared to other treatments, which are markers of late and early T cell activation, respectively (Supporting Information Fig. S4).

3.3. Biodistribution analysis of neoantigen peptides in lymph nodes through locoregional administration

To examine the distribution of peptides, we decorated 10^9 CFU FOLactis with 20 nmol CPP-OVA-CY5 (OVA_{20nmol}-FOLactis-CY5) and measured the peptide signal after one locoregional administration of 20 nmol CPP-OVA-CY5 or OVA_{20nmol}-FOLactis-CY5 in the TDLNs. Near-infrared (NIR) fluorescence imaging was used to assess the fluorescence signal (Fig. 4A). It was apparent that FOLactis could delay the degradation of CPP-OVA-CY5 *in vivo* after injection. And 42.78% fluorescence intensity in the OVA_{20nmol}-FOLactis-CY5 group remained 72 h after the injection, while only 16.10% remained in the CPP-OVA-CY5 group. This contrast became 16.79%−2.60% after 7 d (Fig. 4B). Mice were sacrificed after 72 h and we subsequently collected TDLNs, hearts, livers, spleens, lungs, and kidneys. Compared to the CPP-OVA-CY5 group, the fluorescence of TDLNs in the OVA_{20nmol}-FOLactis-CY5 group was much higher ($P = 0.0057$), potentially presenting a favorable opportunity for antigen recognition and immune activation in TDLNs (Fig. 4C). Furthermore, no significant difference in peptide accumulation was observed in other organs such as livers and kidneys (Fig. 4D).

Considering that the change of immune cells in TDLNs is of great importance, we excised TDLNs and made them into frozen sections 72 h after locoregional injection. As shown in Fig. 4E, the amount of $CD3^+$ and $CD11c^+$ cells treated by OVA_{20nmol}-FOLactis-FAM was much higher than that in the CPP-OVA-FAM group. We observed there was co-localization between immune cells and OVA_{20nmol}-FOLactis-FAM, indicating that FOLactis could attract more DCs to uptake antigens, further activate T cells, and facilitate the communication between T cells and DCs in lymph nodes.

3.4. OVA-bearing FOLactis elicits neoantigen-specific T cells and induces epitope spreading in a subcutaneous melanoma model

To verify the anti-tumor efficacy of FOLactis coated with peptides, we established B16F10-OVA melanoma tumor mouse models by inoculating 2×10^5 tumor cells subcutaneously (Fig. 5A). Three days post-initial inoculation, mice were randomly assigned to four groups: NS group, 20 nmol CPP-OVA, 10^9 CFU FOLactis, and 10^9 CFU FOLactis coated with 20 nmol CPP-OVA (OVA-FOLactis). We dissolved all the drugs in 50 μL NS prior to local administration into the TDLNs. Tumor volumes were recorded every two or three days. We found a significant inhibition of tumor growth in the OVA-FOLactis group during the first two weeks, in comparison to other treatments. The tumor volume of the CPP-OVA group measured 1497.72 mm^3 on Day 18, while that of the OVA-FOLactis group was only 890 mm^3, indicating the great contribution of FOLactis as vectors in modulating immune microenvironment (Fig. 5B and C and Supporting Information Fig. S5). In the NS group and CPP-OVA group, all mice succumbed within 22 days, whereas the survival rate in the OVA-FOLactis group was 70% (Fig. 5D). All groups exhibited a comparable pattern of body weight change throughout the treatment (Supporting Information Fig. S6). Additionally, on the seventh day after the final treatment, we examined H&E-stained images of primary organs, revealing no significant damage across all groups (Supporting Information Fig. S7A). We also detected the liver and kidney functions of the mice in each group. It could be seen that the levels of aspartate aminotransferase (AST), alanine aminotransferase (ALT), alkaline phosphatase (ALP), blood urine nitrogen (BUN), creatinine (CREA) were consistent and within the normal range (Fig. S7B). Due to the potential occurrence of severe side effects during immunotherapy, an evaluation of inflammatory cytokine and chemokine concentrations in the serum was conducted two days post the final treatment. The concentrations of observed IL-2, IL-6, IL-4, IL-10, IL-13, and IL-5 were consistently comparable across all groups, showing no statistically significant differences. This suggests that OVA-FOLactis was well-tolerated (Supporting Information Fig. S8).

Furthermore, we assessed the immune response specific to the antigen in TDLNs and tumors at 7 days post-injection (Fig. 5E and Supporting Information Fig. S9). The proportion of $OVA_{257-264}$ tetramer $^+$ cells in $CD8^+$ T cells in TDLNs in the OVA-FOLactis group (12.002%) was detected about 45-fold higher than NS group (0.264%), and about four-fold higher than the CPP-OVA group (3.216%). Comparable outcomes were observed in the tumors, affirming that OVA-FOLactis triggered a stronger immune response specific to the antigen compared to naked peptides. In order to assess systemic immune activation, we detect the concentrations of IFN-γ and TNF-α in the serum two days after the final treatment. It was shown that increased concentrations of the two inflammatory factors were detected in the OVA-FOLactis group (Supporting Information Fig. S10). The spleen is the

values, while the circle size corresponds to gene correlation ($n = 3$). (F) RNA sequencing was employed to analyze genes associated with the Toll-like receptor signaling pathway or T cell receptor signaling pathway. The high-expression and low-expression genes were grouped through clustering based on $\log_{10}$ (FPKM+1) ($n = 3$).

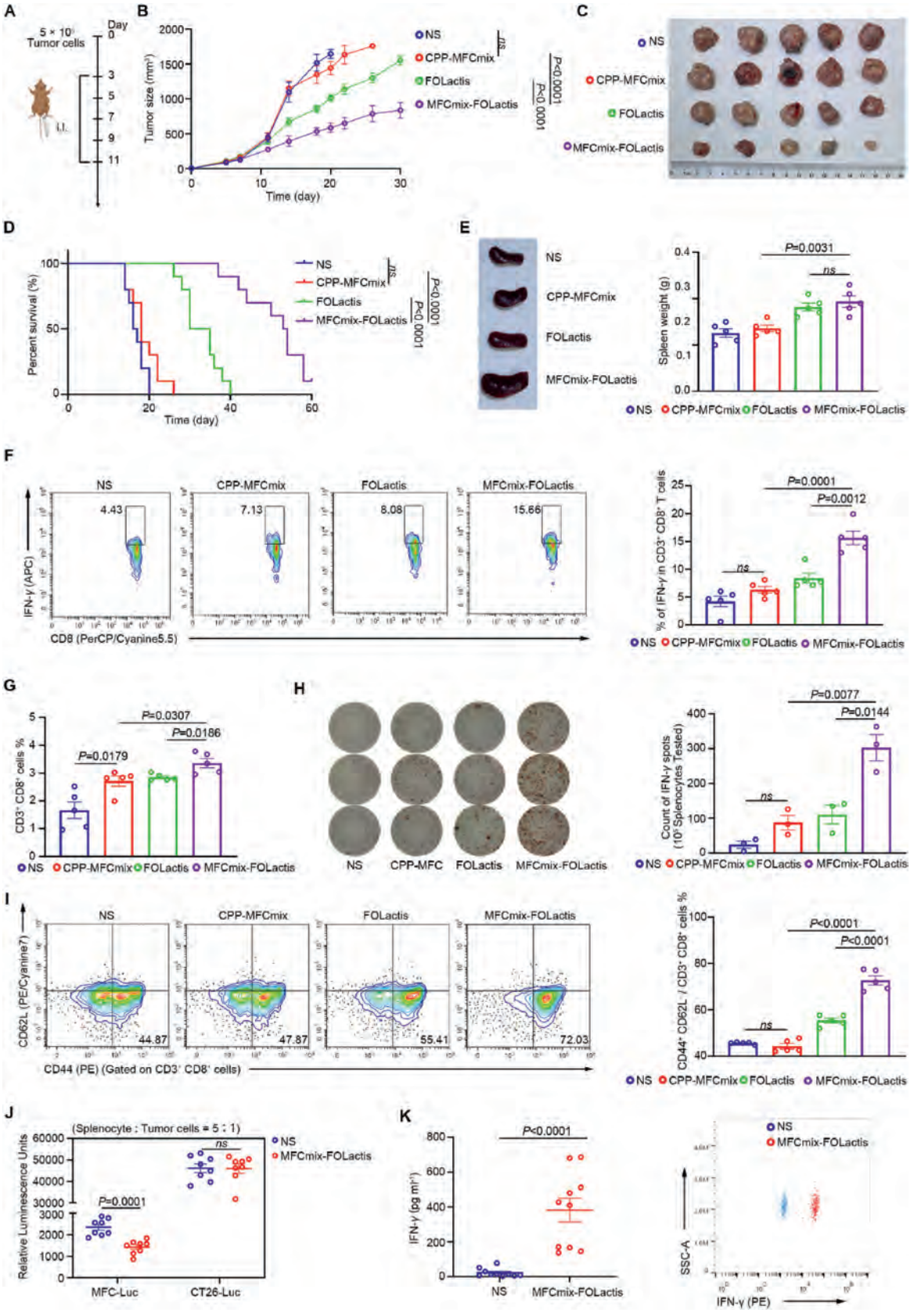

Figure 7 Display of nine tumor antigens by FOLactis generates neoantigen-specific immune memory responses. (A) Illustration depicting the MFC subcutaneous tumor model. 615 mice were injected with 2×10^5 MFC cells subcutaneously and immunized with the following vaccines: normal saline (NS); nine mutant antigens from MFC cells (MFC_{mix}, 10 nmol each peptide); 2×10^9 CFU FOLactis, and 2×10^9 CFU FOLactis coated with nine mutant antigens from MFC cells (10 nmol each peptide) (MFC_{mix}-FOLactis) for five times. Tumor size was assessed starting

major storage site for immune memory cells, so we isolated splenocytes and analyzed the percentages of central memory T cells (T_{CM}) and effector memory T cells (T_{EM}) (Fig. 5F and Supporting Information Fig. S11). In the case of little difference in T_{CM}, the proportion of T_{EM} in the OVA-FOLactis group reached 35.37%, which was significantly higher than the CPP-OVA group. Splenocytes were collected, and the Elispot assay was employed to assess IFN-γ secretion from splenocytes re-stimulated overnight with 10 μmol/L OVA peptide. It was anticipated that splenocytes from mice immunized with OVA-FOLactis demonstrated the highest IFN-γ production compared with other groups (Fig. 5G). Furthermore, the splenocytes extracted from NS-treated and OVA-FOLactis-treated mice were cocultured with CFSE-labeled tumor cells for 6 h (Fig. 5H). The killing effect of splenocytes on B16F10-OVA tumor cells was increased to 49.93% at an effector-to-target ratio (E:T) of 5:1, while the splenocytes exhibited low killing ability on the CT26 tumor cells, showing that OVA-FOLactis induced a specific immune memory response against B16F10-OVA tumors. Notably, the splenocytes in the OVA-FOLactis group could also kill B16F10 tumor cells to a certain degree, suggesting that the memory immune response elicited by OVA-FOLactis was not only limited to administrated neoantigens but also against the other non-immunized neoantigens on B16F10 cells. This phenomenon of epitope spreading further facilitated the progressive development of distinct antitumor immune responses, overcoming immune tolerance amidst selective pressures.

3.5. *OVA-FOLactis reprograms immune microenvironment in TDLNs*

Several studies have shown promising results in utilizing direct injection of antigens/adjuvants into TDLNs for vaccine delivery, enhancing the efficacy of anti-tumor immune agents[23,35,36]. On Day 18, we gathered the TDLNs and observed that they were notably enlarged in the groups immunized with FOLactis or OVA-FOLactis (Fig. 5I). The heightened expression of $CD80^+CD86^+$ suggested an advanced maturation state of DCs, within which the functional $CD103^+$ DCs and $CD8^+$ DCs in the OVA-FOLactis group exhibited more than two-fold increase when contrasted with CPP-OVA group (Fig. 5J−L). We supposed FOLactis could promote the endocytosis and presentation of peptides, and delay their degradation. As expected, the proportion of H-$2K^b$ $OVA_{257\text{-}264}{}^+$ DCs in the OVA-FOLactis group was markedly higher compared to the other three groups (Fig. 5M). Similar findings were found when we detected MHC II^+ DCs in the TDLNs (Fig. 5N). T cells can be stimulated by mature DCs loaded with neoantigens to differentiate into activated subtypes. Furthermore, we examined alterations in T cells within TDLNs. The two groups containing FOLactis exhibited an increase in $CD8^+$ T lymphocytes and a decrease in regulatory T cells (Treg), predicting a favorable immune response (Fig. 5O, P and Supporting Information Fig. S12). Consistently, OVA-FOLactis markedly elevated the percentage of memory T cells (34.5%) and localized concentrations of inflammatory cytokines, including TNF-α and IFN-γ, which acted as the main force to induce effective immune memory and tumor inhibition (Supporting Information Fig. S13).

We also compared OVA-FOLactis with other commonly used antigen adjuvants including ISA51 and Poly-ICLC. It was found that OVA-FOLactis rather than the mixture formulations significantly inhibited the tumor growth and extended the survival time (Supporting Information Fig. S14A−S14C). In the treatment process, the spleens were harvested on Day 18 and further digested into a single-cell suspension for cytometry analysis of immune cell infiltration. As expected, the infiltration of activated and effector memory T cells were all significantly elevated after mice treated with OVA-FOLactis compared to OVA + Poly-ICLC (Fig. S14D−S14F).

3.6. *Both innate and adaptive immunity play essential roles in reshaping the tumor microenvironment*

To explore the mechanisms that contribute to the improved tumor rejection observed after OVA-FOLactis treatment, RNA sequencing (RNA-seq)-based transcriptome analyses of the tumors were performed. In contrast to the NS group, the OVA-FOLactis group exhibited significant up-regulation of 552 genes and down-regulation of 33 genes (Fig. 6A). It was shown in Gene Set Enrichment Analysis (GSEA) that up-regulated genes were mainly related to immune-related response (Fig. 6C and Supporting Information Fig. S15). Gene Ontology (GO) and Kyoto Encyclopedia of Genes and Genomes (KEGG) functional enrichment analyses revealed that OVA-FOLactis significantly upregulated pathways related to the immune system process, inflammatory signaling, and cell chemokines. These pathways included T cell activation, TNF signaling, NF-κB signaling, and so on, which are linked to the stimulation of both innate and adaptive immune responses (Fig. 6B, D, F). The gene network demonstrated that numerous up-regulated genes, especially Tnf, Ifngr1, Tlr9, Tlr2, Cxcl16, Ptprc, and others, played vital roles in promoting immunity, connecting innate immunity with adaptive immunity (Fig. 6E).

DCs and T cells are indispensable for the adaptive immune response, whereas NK cells and macrophages play essential roles

from the initial day of tumor inoculation. Immune responses were analyzed on Day 18. (B) Tumor growth curves were generated for 615 mice subjected to various treatments over a span of 30 days ($n = 7$). Statistics were determined by two-way ANOVA with Tukey's multiple comparisons test. *ns* represented $P > 0.05$. (C) Photos of tumors harvested from mice across all experimental groups on Day 18 (one week following the final treatment) ($n = 5$). (D) Survival trajectories of 615 mice across distinct groups over a 60-day period (n = 10). *P*-values were calculated by log-rank (Mantel-Cox) test. *ns* represented $P > 0.05$. (E) Images of excised spleens showing the splenomegaly and average spleen weight. (F) The proportion of $CD3^+CD8^+$IFN-γ^+ cells in spleens following the vaccination of mice with various drugs ($n = 5$). (G) Flow cytometric examination of $CD3^+CD8^+$ cells in spleens ($n = 5$). (H) The Elispot assay was utilized to assess IFN-γ production by splenocytes following re-stimulation with MFC_{mix} peptide, and the Elispot data underwent quantitative analysis ($n = 3$). (I) Illustrative flow cytometry images and the analysis of T_{EM} in the spleens ($n = 5$). (J) Splenocytes from mice in either the NS or MFC_{mix}-FOLactis group were cultured with MFC-Luc cells or CT26-Luc cells at a ratio of 5:1 for 6 h. Luminescence was measured after adding D-luciferin to the tumor cells ($n = 8$). (K) The IFN-γ concentration in the splenocyte supernatant from 615 mice after co-incubation with MFC-Luc, and representative flow cytometry images ($n = 10$). In all experiments, the error bars represented mean ± SEM. In experiments (E−K), statistical significance was assessed using two-tailed unpaired Student's *t*-test. *ns* represented $P > 0.05$.

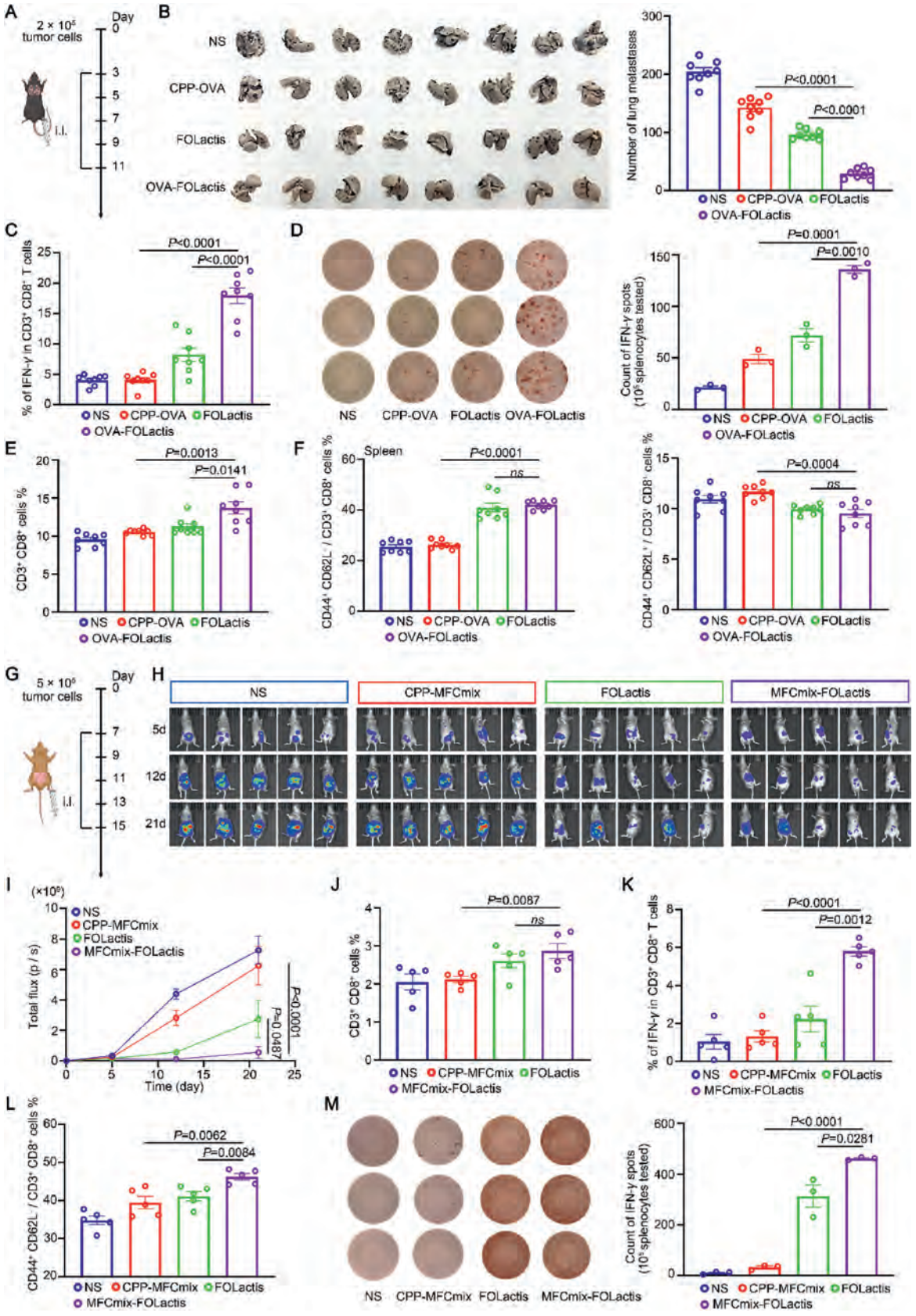

Figure 8 Antitumor effects of neoantigen-bearing FOLactis in metastatic tumor mouse models. (A) Diagram illustrating the B16F10-OVA melanoma lung metastasis mouse model and the treatment schedule for OVA-FOLactis. Mice were intravenously injected with B16F10-OVA melanoma cells ($n = 8$, 2×10^5 cells/mouse) and subsequently vaccinated with the following drugs: normal saline (NS); 20 nmol CPP-OVA;

in innate immunity. We conducted additional assessments of immune cell changes within tumors using flow cytometry assays. It was found that OVA-FOLactis expanded up to 3.50% $CD11c^+CD103^+$ DCs, a 2.1-fold increase compared with CPP-OVA (Supporting Information Fig. S16A). Similarly, the OVA-FOLactis group exhibited approximately a 6.3-fold higher detection of $CD11c^+CD8^+$ DCs compared to the CPP-OVA group (Fig. S16B). The proportion of $CD11c^+MHCII^+$ DCs was also the highest when mice were treated with OVA-FOLactis (Fig. S16C). In contrast to the CPP-OVA group, the OVA-FOLactis group showed a 2.1-fold augmentation in the quantity of $CD8^+$ tumor-infiltrating lymphocytes (TILs), serving as the primary force for direct tumor killing (Fig. S16D and S16G). NK cells are recognized as innate lymphoid cells with formidable cytolytic capabilities, allowing them to detect and eliminate tumor cells directly, independent of antigen presentation[37]. As illustrated in Fig. S16E and S16H, within the tumors at Day 7 post-immunization, the proportion of NK cells increased from 5.48% to 13.68% between the NS group and OVA-FOLactis group. Macrophages comprise a significant portion of tumors, potentially accounting for up to 50% of the tumor mass, exhibiting a high degree of plasticity[38]. We investigated the phenotypic alterations in tumor-associated macrophages (TAMs) following the administration of OVA-FOLactis, which demonstrated a polarization of TAMs from immunosuppressive type 2 (M2) to immune-promoting type 1 (M1) (Fig. S16F).

Reshaping of the tumor immune environment successfully converted the "cold" tumors to "hot", which might be accompanied by an increase of inhibitory molecules like PD-1/PD-L1. Staining of tumors treated with OVA-FOLactis revealed an increased level of PD-1 and PD-L1 expressions (Supporting Information Fig. S17A). Moreover, PD-1 expression on $CD8^+$ TILs in the mice treated with OVA-FOLactis exhibited a notable increase, reaching a 3.33-fold that of the CPP-OVA group (Fig. S17B and S17D). Similarly, PD-L1 expression on tumor cells in mice treated with OVA-FOLactis also demonstrated an elevation, suggesting potential synergistic effects with PD-1 blockade (Fig. S17C and S17D). As depicted in Fig. S17E, mice treated with OVA-FOLactis received intraperitoneal administration of anti-PD1 monoclonal antibody three times to assess the effectiveness of the combination therapy. Though PD-1 alone appeared to show no notable effect on tumor suppression or survival duration, its combination with OVA-FOLactis yielded promising results (Fig. S17F and S17G). It was found that NS-treated and anti-PD1-treated mice died within 21 days, but OVA-FOLactis + anti-PD1 combination therapy increased the percent survival from 0% in OVA-FOLactis to 50% in 60 days (Fig. S17G). The body weights of mice showed no significance across all groups (Fig. S17H).

3.7. Display of nine tumor antigens by FOLactis generates neoantigen-specific immune memory responses

Tumors are inclined to have more than one neoantigen in clinical applications, so it is meaningful if FOLactis can display multiple antigens, which will greatly enhance the versatility of the personalized cancer vaccine platform. To determine the practical feasibility of this concept, we successfully decorated 2×10^9 CFU FOLactis with nine mutant antigens from MFC cells[28] (10 nmol each peptide), that is MFC_{mix}-FOLactis. As described above, we established subcutaneous MFC tumor mouse models and randomly divided them into four groups for local injection of drugs in the TDLNs, including NS, nine mutant antigens from MFC cells (MFC_{mix}, 10 nmol each peptide), 2×10^9 CFU FOLactis, and MFC_{mix}-FOLactis (Fig. 7A). MFC_{mix}-FOLactis resulted in a noteworthy delay in tumor growth compared to alternative treatments, leading to extended survival. Approximately half of the mice survived until Day 53 (Fig. 7B−D). On Day 18, the observed splenomegaly was likely due to the massive proliferation of activated $CD8^+$ T cells in the spleen by MFC_{mix}-FOLactis (Fig. 7E, G). Among the splenic $CD8^+$ T cells, MFC_{mix}-FOLactis prominently enhanced the percentage of IFN-γ-producing $CD8^+$ T cells and T_{EM}, crucially contributing to the initiation of long-term antitumor benefits through immune response activation (Fig. 7F, I). We employed the Elispot assay to measure the secretion of IFN-γ upon restimulation with MFC_{mix} antigen peptides to assess the immune response specific to the antigen in splenocytes. After MFC_{mix}-FOLactis treatment, there was a noteworthy rise in the secretion of peptide-specific IFN-γ by splenocytes, as indicated by the results (Fig. 7H). To further verify the specific tumor-killing ability, splenocytes from MFC-bearing 615 mice, with lysed red blood cells, were co-incubated with MFC-Luc cells or CT26-Luc cells at a ratio of 5:1 for 6 h. Notably, the luciferase activity of MFC-Luc cells greatly decreased when exposed to splenocytes obtained from mice treated with MFC_{mix}-FOLactis (Fig. 7J). The release of IFN-γ in the cell supernatant in the MFC_{mix}-FOLactis group increased by over 17-fold compared to the NS group (Fig. 7K). In contrast, the luciferase activity of CT26-Luc cells showed no significant difference, supposing that MFC_{mix}-FOLactis induced T cells with

10^9 CFU FOLactis; 10^9 CFU FOLactis coated with 20 nmol CPP-OVA (OVA-FOLactis) for five times. We analyzed lung metastasis and immune responses one week after the final treatment. (B) On Day 18, the lungs were harvested, and photographed, and subsequently, we enumerated the tumor nodules of lungs ($n = 8$). (C) Analysis of IFN-γ-secreting $CD3^+CD8^+$ T-cell subpopulation in splenocytes using flow cytometry. (D) Detection of IFN-γ secretion from splenocytes, assessed through the Elispot assay, following re-stimulation with $OVA_{257\text{-}264}$, accompanied by quantitative analysis ($n = 3$). (E−F) Analysis of $CD3^+CD8^+$ cells (E), $T_{EM,}$ and T_{CM} (F) using flow cytometry ($n = 8$). (G) Schematic diagram of the MFC peritoneal metastasis mouse model. 615 mice were administered intraperitoneally with MFC-Luc cells and immunized with the following vaccines: NS; nine mutant antigens from MFC cells (MFC_{mix}, 10 nmol each peptide); 2×10^9 CFU FOLactis, and 2×10^9 CFU FOLactis coated with nine mutant antigens from MFC cells (10 nmol each peptide) (MFC_{mix}-FOLactis) on Days 7, 9, 11, 13, and 15. Analysis of immune responses was conducted on Day 22. ($n = 5$). (H−I) Bioluminescence images depicting tumor burden at Days 5, 12, and 21 post-tumor inoculation ($n = 5$). The displayed images capture the tumor signal (I). (J−L) Flow cytometry analysis of $CD3^+CD8^+$ cells (J), IFN-γ-secreting $CD3^+CD8^+$ T-cell subpopulation (K), and T_{EM} in splenocytes (L) ($n = 5$). (M) The Elispot assay was employed to measure IFN-γ secretion from splenocytes that had undergone re-stimulation with MFC_{mix}, and a quantitative analysis of the Elispot data was conducted ($n = 3$). In all experiments, the error bars represented mean ± SEM. In experiments (B−F, and J−M), statistical significance was determined by analysis of two-tailed unpaired Student's *t*-test. *ns* represented $P > 0.05$. In experiment I, *P*-values were determined by two-way ANOVA with Tukey's multiple comparisons test. *ns* represented $P > 0.05$.

specific killing ability (Fig. 7J). Throughout the treatment, the body weight of mice bearing MFC in all groups remained consistent (Supporting Information Fig. S18). Furthermore, in the MFC_{mix}-FOLactis group, the release of TNF-α and IFN-γ increased by over threefold in contrast to the NS group, while the secretion levels of IL-5, IL-2, IL-6, IL-4, IL-10, and IL-13 remained unchanged, indicating that MFC_{mix}-FOLactis could trigger a systemic immune response against tumors without inducing a severe inflammatory cytokine storm (Supporting Information Fig. S19).

3.8. Antitumor effects of neoantigen-bearing FOLactis in metastatic tumor mouse models

In order to better imitate the diversity of clinical patients and verify the universality of the vaccine platform, we established a mouse model with melanoma lung metastasis and a peritoneal metastasis gastric cancer model. Subsequently, we administered five injections of NS or vaccine formulations to the tumor-bearing mice in the inguinal lymph nodes (Fig. 8A, G). Consistent with the findings in subcutaneous tumor-bearing mouse models, the suppression of tumor progression by OVA-FOLactis or MFC_{mix}-FOLactis was markedly more pronounced in contrast to the other groups (Fig. 8B, H−I).

Spleen, the largest peripheral immune organ in the human body, harbors a significant population of crucial immune cells, notably T cells, essential for coordinating systemic anti-tumor immunity. Thus, we focused on the immune function of mouse splenocytes to investigate the mechanism behind the anti-tumor effect elicited by the vaccine. Compared with naked CPP-peptide, Ag-FOLactis induced a significant increase of $CD3^+$ $CD8^+$ T cells, IFN-γ-secreting $CD3^+$ $CD8^+$ T cells, and T_{EM}, with a slight decrease in the proportion of T_{CM} (Fig. 8C, E−F, J−L, Supporting Information Figs. S20−S22). Furthermore, we employed the Elispot assay to identify neoantigen-specific T cells and observed that splenocytes from mice in the Ag-FOLactis group showed the highest IFN-γ secretion upon restimulation with the corresponding antigen peptide (Fig. 8D, M). The specific killing ability of splenocytes from mice immunized with MFC_{mix}-FOLactis was also analyzed by testing the viability of tumor cells. When the two cells were co-incubated at different times, the results demonstrated that these splenocytes could effectively kill MFC-Luc cells rather than MC38-Luc cells, leading to the increased secretion of IFN-γ (Supporting Information Fig. S23). To conclude, it is worth applying Ag-FOLactis in different tumor-bearing mouse models, which highlights the tremendous clinical translational value of this vaccine platform.

4. Discussions

The rapid evolution of digital-age innovations is driving progress in vaccine development, potentially paving the way for personalized cancer treatment through vaccination tailored to an individual's specific tumor mutations[39]. Emerging data suggest that recognition of tumor neoantigens by T cells can trigger an activated antitumor immune response in patients[40]. However, the immune system's spontaneous processing and presentation of neoantigens is notably inefficient under natural circumstances, which is associated with limited presentation of antigens by DCs, insufficient trafficking to lymphoid organs, and poor immune microenvironment. The most commonly employed strategy to boost the immunogenicity of an antigen is the utilization of adjuvants such as ISA51, alums, and toll-like receptor agonists, aiming to improve the lymph node drainage of the antigen and activate immunity. With the rapid development of synthetic biology and nanomaterials science[41,42], compared with inanimate agents, bacteria which are nature-endowed immune agonists can be genetically engineered by synthetic biology to own a variety of adjuvant functions to better reverse immune escape mechanisms. Among thousands of bacteria, we chose probiotic *Lactococcus lactis* considering its safety and relatively mature genetic toolbox. It produces no endotoxin or exotoxin, making it safer than Gram-negative strains including *Escherichia coli*. The development of NICE® represents a significant advancement in the engineering of *Lactococcus lactis*, affording both precise regulation and increased production of proteins[9,43]. Moreover, *Lactococcus lactis* engineered to secrete IL-10 was the first genetically modified therapeutic bacterium tested in human trials[44]. The FOLactis we designed before was able to sustainably produce Flt3L and OX40L fusion protein, efficiently recruiting cDC1s, drastically increasing cross-presentation, and significantly inducing effector memory T cell activation[13]. Our results showed that FOLactis elicited robust immune adjuvant functions, fostering the maturation of various immune cells and enhancing cytokine release. These effects were attributed to the abundance of pathogen-associated molecular patterns (PAMPs), such as peptidoglycan, and the expression of two immune factors.

Several clinical trials have validated the feasibility of injections into TDLNs[35,45,46]. Ensuring the effective delivery of vaccine components to TDLNs plays a crucial role in inducing strong immune responses since antigens that fail to reach the lymphoid organs could potentially go unrecognized by the immune system, diminishing their impact[47]. It has been revealed that incorporating soluble antigen/adjuvant or alum formulations in conjunction with nanoparticles of appropriate size increases the likelihood of transporting vaccine components to lymphoid organs. However, it is important to note that despite these advancements, a significant portion of the injected material still tends to accumulate at the vaccination site, rendering it functionally ineffective in stimulating the immune response[48,49]. Therefore, i.DN injection directly delivers the entire vaccine to the site where the initial immune response is triggered, thereby maximizing the response per dose. Apart from the physical location, it is crucial to take into account the timing of the immune system's encounter with a vaccine to achieve the highest level of protective immunity. Recent studies examining the influence of antigen and adjuvant kinetics on T-cell responses indicate that maintaining the immune system's exposure to both antigen and adjuvant molecules over several days enhances the immunogenicity of the vaccine[25-27,50,51]. Nevertheless, naked antigen peptides are always rapidly cleared from the body.

To better improve the delivery of vaccines to TDLNs and sustain the exposure time of antigens, we combined the two approaches. We decorated FOLactis with CPP-peptides and directly injected them into TDLNs. Our results proved that i.DN with Ag-FOLactis allows longer storage time of neoantigen peptides in TDLNs, which would give them more time to be taken up by DCs, subsequently initiating T cell responses. Employing two different mouse models of B16F10-OVA and MFC treated with the corresponding Ag-FOLactis, respectively, we found robust infiltration of antigen-specific T cells in the TDLNs, tumors, and spleens, leading to the significant tumor inhibition and longer survival periods of mice. More importantly, i.DN with Ag-FOLactis could reprogram both TDLN and tumor immune microenvironment without causing severe systemic side effects, which was able to

convert "cold" tumors to "hot". To be more specific, Ag-FOLactis was also observed to deflect M2 to M1 macrophages, impact various immune cell types such as Tregs and NKs, trigger heightened lymphocyte cytotoxicity, and elevate the levels of several vital cytokines. Immune tolerance stands as another crucial factor constraining the effectiveness of immunotherapy. A typical illustration of this is the weariness of T cells, which occurs alongside the increased expression of PD-1 following immunotherapy. It was shown that Ag-FOLactis had a synergistic effect with PD1. Additionally, tumor antigen expression will undergo Darwinian evolution under the selection pressure of neoantigen-reactive T cells, contributing to the new genomic mutations[52]. Notably, splenocytes of mice treated with OVA-FOLactis had the killing ability not only to B16F10-OVA cells but also to B16F10 cells. This epitope-spreading effect might be due to the antitumor immune cycle formed by the long-lasting immune-stimulating effect of the engineered probiotic neoantigen platform.

In terms of how to load FOLactis with tumor neoantigens, it is necessary to find a convenient and efficient strategy. The CPP sequence was fused to the N-terminus of the tumor epitopes as an attachment moiety, which facilitated stable coating with FOLactis without affecting the presentation of these peptides. Compared with other complex chemical methods which might bring a variety of chemical reagents[53-55] to the surface of bacteria, our strategy could be easier and safer. Moreover, the diversity of neoantigens within and across tumor cells highlights the necessity for a swift antigen display technology in tumor vaccines. We employed the Plug-and-Display technology to prepare Ag-FOLactis, with the vector and antigen separately synthesized, which required only a simple combination procedure before immunization. Whether it is one or more antigens, it can be effectively decorated on the FOLactis. Meanwhile, we could produce different engineered *Lactococcus lactis* to meet clinical needs and establish a neoantigen library in advance. These off-the-shelf components remarkably reduce the production time, laying the groundwork for the future on-demand production of personalized tumor vaccines tailored to individual patients.

Some limitations still existed in our study. Though Ag-FOLactis induced significantly increased antigen-specific T-cell responses, the effect on tumor growth control did not come up to expectations. Exploring the molecular aspect of this phenomenon in the future is of great value for us and it is meaningful to try different combination strategies. Considering patient compliance, it might be worthwhile to encapsulate Ag-FOLactis in biological materials such as hydrogel and reduce dosing frequency.

5. Conclusions

Overall, we designed an engineered *Lactococcus lactis*-based personalized cancer vaccine platform, which brings the advantages of synthetic biology, bacteriology, and immunology together. We believe that Ag-FOLactis provides a broad possibility for further clinical promotion and precision medicine.

Acknowledgments

This work was financially supported by the National Natural Science Foundation of China (81930080 and 82272811), the Fund for Distinguished Young Scholars of Jiangsu Province (BK20230001, China), and the Key Project Foundation of Nanjing for the Development of Medical Technology (ID: ZKX20024, China).

Author contributions

Junmeng Zhu: Writing − original draft, Validation, Software, Project administration, Methodology, Formal analysis, Data curation. Yi Sun: Software, Methodology, Data curation. Xiaoping Qian: Software, Methodology, Data curation. Lin Li: Software, Methodology. Fangcen Liu: Software, Methodology. Xiaonan Wang: Software, Methodology. Yaohua Ke: Software, Data curation. Jie Shao: Methodology, Data curation. Lijing Zhu: Software, Methodology. Lifeng Wang: Software, Data curation. Qin Liu: Supervision, Project administration, Methodology, Investigation, Data curation. Baorui Liu: Validation, Supervision, Resources, Project administration, Investigation, Funding acquisition, Conceptualization.

Conflicts of interest

The authors have no conflicts of interest to declare.

Appendix A. Supporting information

Supporting information to this article can be found online at https://doi.org/10.1016/j.apsb.2025.02.041.

References

1. Blass E, Ott PA. Advances in the development of personalized neoantigen-based therapeutic cancer vaccines. *Nat Rev Clin Oncol* 2021;**18**:215−29.
2. Peres C, Matos AI, Moura LIF, Acúrcio RC, Carreira B, Pozzi S, et al. Preclinical models and technologies to advance nanovaccine development. *Adv Drug Deliv Rev* 2021;**172**:148−82.
3. Schlom J, Gulley JL. Vaccines as an integral component of cancer immunotherapy. *Jama* 2018;**320**:2195−6.
4. Melssen MM, Fisher CT, Slingluff CL, Melief CJM. Peptide emulsions in incomplete Freund's adjuvant create effective nurseries promoting egress of systemic $CD4^+$ and $CD8^+$ T cells for immunotherapy of cancer. *J Immunother Cancer* 2022;**10**:e004709.
5. Liu T, Zhu M, Chang X, Tang X, Yuan P, Tian R, et al. Tumor-specific photothermal-therapy-assisted immunomodulation *via* multi-responsive adjuvant nanoparticles. *Adv Mater* 2023;**35**:e2300086.
6. Zhao X, Chen X, Yuk H, Lin S, Liu X, Parada G. Soft materials by design: unconventional polymer networks give extreme properties. *Chem Rev* 2021;**121**:4309−72.
7. Li J, Xia Q, Guo H, Fu Z, Liu Y, Lin S, et al. Decorating bacteria with triple immune nanoactivators generates tumor-resident living immunotherapeutics. *Angew Chem Int Ed Engl* 2022;**61**:e202202409.
8. Liu Y, Zhang M, Wang X, Yang F, Cao Z, Wang L, et al. Dressing bacteria with a hybrid immunoactive nanosurface to elicit dual anticancer and antiviral immunity. *Adv Mater* 2023;**35**:e2210949.
9. Kuipers OP, Beerthuyzen MM, de Ruyter PG, Luesink EJ, de Vos WM. Autoregulation of nisin biosynthesis in *Lactococcus lactis* by signal transduction. *J Biol Chem* 1995;**270**:27299−304.
10. Jin SW, Lee GH, Jang MJ, Hong GE, Kim JY, Park GD, et al. Immunomodulatory activity of *Lactococcus lactis* GCWB1176 in cyclophosphamide-induced immunosuppression model. *Microorganisms* 2020;**8**:1175.
11. Kaczmarek K, Więckiewicz J, Węglarczyk K, Siedlar M, Baran J. The anti-tumor effect of *Lactococcus lactis* bacteria-secreting human soluble TRAIL can be enhanced by metformin both *in vitro* and *in vivo* in a mouse model of human colorectal cancer. *Cancers (Basel)* 2021;**13**:3004.
12. Garbacz K. Anticancer activity of lactic acid bacteria. *Semin Cancer Biol* 2022;**86**:356−66.

13. Zhu J, Ke Y, Liu Q, Yang J, Liu F, Xu R, et al. Engineered *Lactococcus lactis* secreting Flt3L and OX40 ligand for *in situ* vaccination-based cancer immunotherapy. *Nat Commun* 2022;**13**:7466.
14. Murciano-Goroff YR, Warner AB, Wolchok JD. The future of cancer immunotherapy: microenvironment-targeting combinations. *Cell Res* 2020;**30**:507−19.
15. Böttcher JP, Bonavita E, Chakravarty P, Blees H, Cabeza-Cabrerizo M, Sammicheli S, et al. NK cells stimulate recruitment of CDC1 into the tumor microenvironment promoting cancer immune control. *Cell* 2018;**172**:1022−37.e14.
16. Roberts EW, Broz ML, Binnewies M, Headley MB, Nelson AE, Wolf DM, et al. Critical role for $CD103^+$/$CD141^+$ dendritic cells bearing CCR7 for tumor antigen trafficking and priming of T Cell immunity in melanoma. *Cancer Cell* 2016;**30**:324−36.
17. Enamorado M, Iborra S, Priego E, Cueto FJ, Quintana JA, Martínez-Cano S, et al. Enhanced anti-tumour immunity requires the interplay between resident and circulating memory $CD8^+$ T cells. *Nat Commun* 2017;**8**:16073.
18. du Bois H, Heim TA, Lund AW. Tumor-draining lymph nodes: at the crossroads of metastasis and immunity. *Sci Immunol* 2021;**6**:eabg3551.
19. Loo CP, Nelson NA, Lane RS, Booth JL, Loprinzi Hardin SC, Thomas A, et al. Lymphatic vessels balance viral dissemination and immune activation following cutaneous viral infection. *Cell Rep* 2017;**20**:3176−87.
20. Lund AW, Wagner M, Fankhauser M, Steinskog ES, Broggi MA, Spranger S, et al. Lymphatic vessels regulate immune microenvironments in human and murine melanoma. *J Clin Investig* 2016;**126**:3389−402.
21. Poggio M, Hu T, Pai CC, Chu B, Belair CD, Chang A, et al. Suppression of exosomal PD-L1 induces systemic anti-tumor immunity and memory. *Cell* 2019;**177**:414−27.e13.
22. Schudel A, Francis DM, Thomas SN. Material design for lymph node drug delivery. *Nat Rev Mater* 2019;**4**:415−28.
23. Francis DM, Manspeaker MP, Schudel A, Sestito LF, O'Melia MJ, Kissick HT, et al. Blockade of immune checkpoints in lymph nodes through locoregional delivery augments cancer immunotherapy. *Sci Transl Med* 2020;**12**:eaay3575.
24. Pape KA, Catron DM, Itano AA, Jenkins MK. The humoral immune response is initiated in lymph nodes by B cells that acquire soluble antigen directly in the follicles. *Immunity* 2007;**26**:491−502.
25. Bachmann MF, Beerli RR, Agnellini P, Wolint P, Schwarz K, Oxenius A. Long-lived memory $CD8^+$ T cells are programmed by prolonged antigen exposure and low levels of cellular activation. *Eur J Immunol* 2006;**36**:842−54.
26. Prlic M, Hernandez-Hoyos G, Bevan MJ. Duration of the initial TCR stimulus controls the magnitude but not functionality of the $CD8^+$ T cell response. *J Exp Med* 2006;**203**:2135−43.
27. Johansen P, Storni T, Rettig L, Qiu Z, Der-Sarkissian A, Smith KA, et al. Antigen kinetics determines immune reactivity. *Proc Natl Acad Sci U S A* 2008;**105**:5189−94.
28. Liu Q, Chu Y, Shao J, Qian H, Yang J, Sha H, et al. Benefits of an immunogenic personalized neoantigen nanovaccine in patients with high-risk gastric/gastroesophageal junction cancer. *Adv Sci* 2022;**10**:e2203298.
29. Jewell CM, López SC, Irvine DJ. *In situ* engineering of the lymph node microenvironment *via* intranodal injection of adjuvant-releasing polymer particles. *Proc Natl Acad Sci USA* 2011;**108**:15745−50.
30. Harrell MI, Iritani BM, Ruddell A. Lymph node mapping in the mouse. *J Immunol Methods* 2008;**332**:170−4.
31. Martínez B, Rodríguez A, Kulakauskas S, Chapot-Chartier MP. Cell wall homeostasis in lactic acid bacteria: threats and defences. *FEMS Microbiol Rev* 2020;**44**:538−64.
32. Wculek SK, Cueto FJ, Mujal AM, Melero I, Krummel MF, Sancho D. Dendritic cells in cancer immunology and immunotherapy. *Nat Rev Immunol* 2020;**20**:7−24.
33. Kobayashi E, Jin A, Hamana H, Shitaoka K, Tajiri K, Kusano S, et al. Rapid cloning of antigen-specific T-cell receptors by leveraging the cis activation of T cells. *Nat Biomed Eng* 2022;**6**:806−18.
34. Zhao Y, Caron C, Chan YY, Lee CK, Xu X, Zhang J, et al. cis-B7:CD28 interactions at invaginated synaptic membranes provide CD28 co-stimulation and promote $CD8^+$ T cell function and anti-tumor immunity. *Immunity* 2023;**56**:1187−203.e12.
35. Senti G, Johansen P, Kündig TM. Intralymphatic immunotherapy. *Curr Opin Allergy Clin Immunol* 2009;**9**:537−43.
36. Johansen P, Häffner AC, Koch F, Zepter K, Erdmann I, Maloy K, et al. Direct intralymphatic injection of peptide vaccines enhances immunogenicity. *Eur J Immunol* 2005;**35**:568−74.
37. Deng W, Gowen BG, Zhang L, Wang L, Lau S, Iannello A, et al. Antitumor immunity. A shed NKG2D ligand that promotes natural killer cell activation and tumor rejection. *Science* 2015;**348**:136−9.
38. Hu G, Guo M, Xu J, Wu F, Fan J, Huang Q, et al. Nanoparticles targeting macrophages as potential clinical therapeutic agents against cancer and inflammation. *Front Immunol* 2019;**10**:1998.
39. Sahin U, Türeci Ö. Personalized vaccines for cancer immunotherapy. *Science* 2018;**359**:1355−60.
40. Schumacher TN, Schreiber RD. Neoantigens in cancer immunotherapy. *Science* 2015;**348**:69−74.
41. Wanderi K, Cui Z. Organic fluorescent nanoprobes with NIR-IIb characteristics for deep learning. *Explor (Beijing)* 2022;**2**:20210097.
42. Feng C, Tan P, Nie G, Zhu M. Biomimetic and bioinspired nanoplatforms for cancer vaccine development. *Explor (Beijing)* 2023;**3**:20210263.
43. Mierau I, Olieman K, Mond J, Smid EJ. Optimization of the *Lactococcus lactis* nisin-controlled gene expression system NICE for industrial applications. *Microb Cel Fact* 2005;**4**:16.
44. Braat H, Rottiers P, Hommes DW, Huyghebaert N, Remaut E, Remon JP, et al. A phase I trial with transgenic bacteria expressing interleukin-10 in Crohn's disease. *Clin Gastroenterol Hepatol* 2006;**4**:754−9.
45. Senti G, Prinz Vavricka BM, Erdmann I, Diaz MI, Markus R, McCormack SJ, et al. Intralymphatic allergen administration renders specific immunotherapy faster and safer: a randomized controlled trial. *Proc Natl Acad Sci U S A* 2008;**105**:17908−12.
46. Weber J, Boswell W, Smith J, Hersh E, Snively J, Diaz M, et al. Phase 1 trial of intranodal injection of a Melan-A/MART-1 DNA plasmid vaccine in patients with stage IV melanoma. *J Immunother* 2008;**31**:215−23.
47. Zinkernagel RM, Ehl S, Aichele P, Oehen S, Kündig T, Hengartner H. Antigen localisation regulates immune responses in a dose- and time-dependent fashion: a geographical view of immune reactivity. *Immunol Rev* 1997;**156**:199−209.
48. Reddy ST, van der Vlies AJ, Simeoni E, Angeli V, Randolph GJ, O'Neil CP, et al. Exploiting lymphatic transport and complement activation in nanoparticle vaccines. *Nat Biotechnol* 2007;**25**:1159−64.
49. Manolova V, Flace A, Bauer M, Schwarz K, Saudan P, Bachmann MF. Nanoparticles target distinct dendritic cell populations according to their size. *Eur J Immunol* 2008;**38**:1404−13.
50. Yang Y, Huang CT, Huang X, Pardoll DM. Persistent Toll-like receptor signals are required for reversal of regulatory T cell-mediated CD8 tolerance. *Nat Immunol* 2004;**5**:508−15.
51. Shaulov A, Murali-Krishna K. CD8 T cell expansion and memory differentiation are facilitated by simultaneous and sustained exposure to antigenic and inflammatory milieu. *J Immunol* 2008;**180**:1131−8.
52. Meneveau MO, Petroni GR, Salerno EP, Lynch KT, Smolkin M, Woodson E, et al. Immunogenicity in humans of a transdermal multipeptide melanoma vaccine administered with or without a TLR7 agonist. *J Immunother Cancer* 2021;**9**:e002214.
53. Dong X, Pan P, Ye JJ, Zhang QL, Zhang XZ. Hybrid M13 bacteriophage-based vaccine platform for personalized cancer immunotherapy. *Biomaterials* 2022;**289**:121763.
54. Jing Z, Wang S, Xu K, Tang Q, Li W, Zheng W, et al. A potent micron neoantigen tumor vaccine GP-neoantigen induces robust antitumor activity in multiple tumor models. *Adv Sci* 2022;**9**:e2201496.
55. Pan C, Li J, Hou W, Lin S, Wang L, Pang Y, et al. Polymerization-mediated multifunctionalization of living cells for enhanced cell-based therapy. *Adv Mater* 2021;**33**:e2007379.